

## Revision 2

# **Mannardite as the main vanadium-hosting mineral in black shale-hosted vanadium deposits, South China**

LIFEI YANG<sup>1,2</sup>, ZENGHUA LI<sup>1\*</sup>, YONGPENG OUYANG<sup>3\*</sup>, TENG DENG<sup>1</sup>,

YOUGUO DENG<sup>3</sup>, DERU XU<sup>1</sup>

<sup>1</sup> State Key Laboratory for Nuclear Resources and Environment, East China University of Technology, Nanchang, Jiangxi 330013, China

<sup>2</sup> School of Marine Engineering, Jiujiang Vocational and Technical College, Jiujiang, Jiangxi 332007, China

<sup>3</sup> The Tenth Geological Brigade of Jiangxi Geological Bureau, Yingtan, Jiangxi 335001, China

\*Corresponding author: ZENGHUA LI ([lizenghua@ecut.edu.cn](mailto:lizenghua@ecut.edu.cn)); YONGPENG

OUYANG ([yongpeng0524@163.com](mailto:yongpeng0524@163.com))

## **ABSTRACT**

Black shale-hosted vanadium (V) deposits accounts for about 80% vanadium resource in the world, but only less than 2% vanadium in the black shale can be extracted mainly due to insufficient recognition on the occurrence mode of vanadium. It is commonly agreed that most vanadium in the black shale is hosted in clay minerals and organic matters, but it is not clear how the other parts of vanadium exist and whether there is vanadium mineral, which limits the understanding of metallogenic mechanism of black shale-hosted vanadium

deposit. The Jiujiang Basin at the Lower Yangtze Block is a significant black shale-hosted vanadium metallogenic district. In this research, systematic studies of mineralogy, crystallography, lithology and geochemistry from two deposits were conducted to confirm the occurrence of vanadium hosted in the black shales. Results from electron probe micro analysis (EPMA), Raman spectrum and in-situ XRD suggest that the main vanadium-hosting mineral in the black shale is mannardite, with a crystallochemistry formula of  $[\text{Ba}_{0.96} \cdot \text{H}_2\text{O}] (\text{Ti}_{5.87} \text{V}^{3+}_{1.87} \text{V}^{4+}_{0.11} \text{Si}_{0.07} \text{Cr}_{0.07} \text{Fe}^{3+}_{0.02}) \text{O}_{16.00}$ , space group  $I4_1/a$ , cell parameters  $a = b = 14.346(7) \text{ \AA}$ ,  $c = 5.899(1) \text{ \AA}$ ,  $\alpha = \beta = \gamma = 90^\circ$ ,  $Z = 4$ . Data from electron probe micro analysis (EPMA), tescan integrated mineral analyzer (TIMA) and whole-rock geochemistry indicate that 12.32%–44.06% (average of 24.95%) vanadium exists in mannardite. The crystallochemistry formula in this research suggests that main vanadium in the mannardite occupies stable crystallographic locations as trivalent vanadium ( $\text{V}^{3+}$ ), forming chemical bonds with oxygen atom by  $\text{VO}_2^-$ , whereas minor vanadium replaces titanite atom ( $\text{Ti}^{4+}$ ) as quadrivalent vanadium ( $\text{V}^{4+}$ ) by isomorphism. Mannardite precipitates under a strong reductive condition with sufficient trivalent vanadium species, titanium (Ti) and biogenic barium (bio-barite). The first identification of mannardite in black shales-hosted vanadium deposits puts forward new cognition on occurrence mode of vanadium and the metallogenic mechanism of the black shale-hosted vanadium deposit. Besides, the mannardite provides mineralogical support for the beneficiation of vanadium from the black shale.

**Keywords:** Black shale-hosted vanadium deposit, mannardite, occurrence mode, metallogenic mechanism, Jiujiang Basin, South China

## INTRODUCTION

Vanadium is widely used in industries of steel, alloys, aviation, petrochemical engineering and energy storage (Dang et al. 2018; Ettler et al. 2020). It has been classified as critical metal by the European Union and American (Schulz et al. 2017; EC, 2018; Bai et al. 2021). The data from USGS (2022) and Zhang et al. (2011) show that about 80% vanadium is hosted in the black shale-hosted deposit, which is mainly distributed in South China (Fig. 1a; Zhang et al. 2011; Liu et al. 2019a; Yang et al. 2022). This type of vanadium deposits is characterized with large reserves and high grade (118 million tons  $V_2O_5$  with mainly grade of 0.5–1.7 wt%), comparing with the Fe-Ti-V deposits (17.6 million tons  $V_2O_5$  with grade of 0.2 wt%; Cao et al. 2019; Villanova-de-Benavent et al. 2017; Zhang et al. 2011, 2017). However, less than 2% vanadium is obtained from the black shale-hosted vanadium deposits (Wang and Ma 2009), due to insufficient recognition on the mineral constituent, occurrence mode of vanadium in the black shale (Zhang et al. 2011, 2015, 2017; Wang et al. 2017; Zhu et al. 2018), which also limits the understanding on vanadium metallogenic mechanism.

The vanadium minerals in the vanadium deposits are the direct evidence on understanding the metallogenic conditions and the accumulation mechanism of vanadium. It has been confirmed that vanadium minerals can formed on vavrious conditions and exist

in the vanadiferous titanomagnetite deposits (coulsonite; Karpov et al. 2012), sandstone type vanadium deposit (carnotite, corvusite, doloresite, hewettite, paramontroseite; Henderson and Hess 1933; Garrels et al. 1956; Wülser et al. 2011; Schmid et al. 2020), vanadate deposits (descloizite, mottramite and vanadinite; Boni et al. 2007; Sracek et al. 2014) and hydrothermal metal deposit (karelianite, nolanite, schreyerite, vanadium andradite, shcherbinaite; Howard and Owens 1995; Spry and Scherbarth 2006; Sergeeva et al. 2011). However, vanadium mineral constituent in the black shale-hosted vanadium deposit has kept blank. Previous studies indicate that the occurrences of vanadium includes adsorbing on the surface of ferric and aluminum oxides (Micera and Dallochio 1988; Peacock and Sherman, 2004; Zhu et al. 2018), enriching in clay minerals by isomorphism (Peacock and Sherman 2004; Zhang et al. 2015; Wang et al. 2017; Zhou et al. 2020) and occurring in vanadium-organic compounds (Maylotte et al. 1981; Mercer et al. 1992; Gol'dberg et al. 2010). However, only less than 2% vanadium in the black shale can be extracted, which is due to the difficulty of extracting micro clay minerals from black shale and the indistinct occurrence modes (Xue et al. 2021b).

The Jiujiang Basin at the South China Craton is an important vanadium metallogenic zone, and hosts a number of black shale-hosted vanadium deposits (Zhou et al. 2019; Li et al. 2022a; Yang et al. 2022). In this study, systematic mineralogy, crystallography and geochemistry analysis of the Yangjiashan and Liujiqiao deposits are conducted to examine the occurrence mode of vanadium. Based on the results, the precipitation

machanism of vanadium in the black shale is dicussed, providing mineralogical support for the extracting of vanadium from the black shale.

## **GEOLOGICAL SETTING**

The Jiujiang region is tectonically located at the Lower Yangtze Block (Fig. 1; Chen et al. 1991; Li et al. 2003b, 2010; Liu et al. 2011; Qian and Wei 2019; Zhao 2020; Kan et al. 2022). During Early Tonian, the Jiujiang region developed into active continental margin due to the shrink of the South China Ocean, which lead to the deposition of bathyal-abyssal-neritic facies of the Hengyong Formation and development of Jiujiang back-arc basin (Fig. 1b; Chen et al. 1991; Cai and Gu 2002; Li et al. 2003a, 2010; Yang et al. 2015). During Late Tonian–Ediacaran, the Jiujiang epicontinental ocean basin formed and kept stable until Silurian, which resulted from the extensional setting of the Lower Yangtze Block (Yang 2011; Sracek et al. 2014). As results, the Jiujiang Basin received the Cryogenian continental facies (including sandstone, tuff, glutenite, tillite) and the Ediacaran neritic facies (Fig. 1b).

During the epicontinental ocean basin phase, Early Paleozoic sediments distribute extensively at the Jiujiang Basin (JGSEI 2017). The Cambrian strata consists of the lower shale and upper limestone (Fig. 1b). Especially, the black carbonaceous shale, carbon siliceous shale from the Hetang and Guanyintang formations inherits from the Ediacaran sediments. The plenty of organic carbon in the Hetang Formation black shale indicates that this stratum constitutes the unique abysmal basin facies and sedimented under a reductive

environment in the Jiujiang epicontinental ocean basin, which was resulted from the microorganism teeming after glacial epoch during Cryogenian (Zhou 1990; Wang et al. 2013; Tang et al. 2017). During the late period of Early Cambrian, the sea level dropped rapidly, and the Jiujiang Basin evolved from abysmal environment into epeiric sea continental shelf settings, resulting in existence of shallow color arenaceous shale and siltstone with plenty of trilobite in the Guanyintang Formation (Wan 2010; Wang et al. 2013). The Yangliugang Formation of Lower Cambrian consists of the lower tidal-flat facies calcareous dolomite at and the upper spacious platform facie argillaceous limestone with trilobite, indicating the sea level increased. During Late Cambrian, this platform environment developed into tidal-flat-lagoonal setting, which kept stable till Early Silurian (Liu et al. 2011). As results, the Jiujiang Basin received the argillaceous-dolomitic limestone of the Huayansi, Xiyangshan formations, tidal-flat carbonate strata of the Cangshan Formation and sandstone-arenaceous shale-graywacke of the Lishuwo Formation (Kan et al. 2022). Experiencing a long history of epicontinental ocean basin phase, the crust uplifted at Jiujiang region resulted from the orogenesis and close of the South China Ocean again during Middle Silurian (Wang et al. 2020). Consequently, minor fragmentary epeiric sea facies existed, including the Upper Silurian Xiajiaqiao, Xikeng formations and the Devonian Wutong Formation. The South China Ocean extended once again since Late Carboniferous, generating limestone and dolostone system-the epeiric sea facies (Fig. 1b).

During the evolution of Lower Yangtze Block, the Jiujiang Basin remained stable during Early Cambrian. The persistent and stable reduced sedimentary environment in Jiujiang Basin provides significant condition for the formation of sedimentary vanadium deposits (Fig. 1b; Qian and Wei 2019; Zhou et al. 2019; Li et al. 2022b).

The structures at Jiujiang Basin exhibit NE direction. The folds mainly existed in the strata after Ediacaran, involving NNE synclinalia and NE anticline. Besides, the fault zone consists of dextral NE faults through the overlay strata (Fig. 1b).

### **DEPOSIT GEOLOGY**

At the Yangjiashan deposit, the sediments system in the ore field comprises the Late Ediacaran, Early Cambrian and the Quaternary strata (Figs. 2a–b). The Ediacaran Piyuancun Formation (about 400 m thick) consists of black gray massive pyrite-bearing silicalite, dark gray carbonaceous silicalite and microcrystalline limestone, a bottom-up sequence that exhibits property of sub-abyssal basin facies (Figs. 2a–b). The Early Cambrian Hetang Formation consists of unique abyssal basin sequences under an anoxic environment and is rich in vanadium, and a 30 m thick stone coal layer with black pyrite-bearing carbon siliceous shale and pyrite-bearing carbonaceous shale exist at the bottom, (Figs. 4b, d–e). The overlying strata is carbon siliceous shale within thin carbonaceous shale (Figs. 4c and f). The upper part of Hetang Formation is the black carbonaceous silicalite with interlayer of carbonaceous shale (Fig. 4a). From geological outcrop, slight deformation and metamorphism happen to the Hetang Formation, resulting in the existence

of minor carbonatite veinlet (Figs. 4b, f). The Hetang Formation contact conformably with the Piyuncun Formation at the bottom and the overlying Guangyintang Formation (Fig. 4a). Due to the reduce of sea level, the Jiujiang region developed into epeiric continental shelf basin at the late period of Early Cambrian. As a result, light gray argillaceous and silt shale of the Guanyintang Formation deposited (Fig. 4a). The Quaternary strata mainly includes yellowish-brown clay and glutenite along the Yangtze River (Fig. 1b). No magmatism and volcanism occur in the ore filed.

The Liujiqiao vanadium deposit shares similar sedimentary sequences with the Yangjiashan deposit (Fig. 3).

In the Yangjiashan deposit, total twelve vanadium ore bodies have been identified (Fig. 2b). These ore bodies are mainly hosted in carbonaceous shales and pyrite-bearing carbon siliceous shales of the lower sequence of the Hetang Formation. Minor ore body also occur on the top of the Piyuncun Formation. Generally, the ore bodies are bedded, dip to  $120^{\circ}$ – $250^{\circ}$  with dip angle varies during  $10$ – $35^{\circ}$ , consistent with the host rocks, which suggests the black shale of the Hetang Formation is the significant ore-controlling factors. The  $V_2O_5$  grade ranges from 0.70 wt% to 0.89 wt% (Zhao 2020). The ore bodies of  $V_4$ ,  $V_5$  and  $V_8$  contribute most of vanadium resource for the Yangjiashan deposit (Fig. 2b).

Similar to the Yangjiashan deposit, twelve ore bodies have been prospected in the Liujiqiao deposit, of which four ore bodies can be observed along the exploration line 8 (Fig. 3b). All the ore bodies exhibit same attitude to the Hetang Formation as stratiform,

stratiform-like and lensoid with 600–810 m long, 1.15–13.5 m thick and 0.70–1.06 wt% V<sub>2</sub>O<sub>5</sub>. The vanadium mainly accumulates at the black carbonaceous shale and black carbon siliceous shale, in which pyrite exists pervasively.

## **SAMPLING AND ANALYTICAL METHODS**

### **Sampling**

The samples are collected from the outcrop and the cores of the two deposits, and the detail locations are shown in the figures 2 and 3. Total 13 samples are collected from the Hetang Formation, including 8 ore samples hosted in black carbon siliceous shale (samples SHAD, D11, D15, D21; ZK801D7, D12, D27, D29) and 5 ore samples hosted in the black carbonaceous shale (ZK801D14, D15, D21, D32, D40).

### **Electron probe micro analysis (EPMA)**

Mineral compositions are obtained by using electron probe micro analysis (EPMA) at the State Key Laboratory of Nuclear Resource and Environment, East China University of Technology, with a JEOL JXA-8230 Electron Probe Micro Analyzer equipped with four wavelength-dispersive spectrometers. Before the analysis by EPMA, thin sections of samples were polished and coated with a thin conductive carbon film. During the analysis, an accelerating voltage of 15 kV, a beam current of 20 nA and a 1 μm spot size were used to analyse minerals. Data were corrected on-line using a modified ZAF (atomic number, absorption, fluorescence) correction procedure. The peak counting time was 10 s for Ba, V, Ti, Na, K, Mg, Al, Si, Ca, Fe, S, As, F and 20 s for Cr, Zn, Ni, Sr and Mn. The background counting time was one-half of the peak counting time on the high- and low-energy

background positions. The standard minerals in this research include biotite ( $K_2O$ ), rutile ( $TiO_2$ ), jadeite ( $Na_2O$ ), tugtupite (Cl), fluorite (F), olivine (FeO), anhydrite ( $SO_3$ ), barite ( $BaO$ ), plagioclase (CaO), chromium oxide ( $Cr_2O_3$ ),  $V(V_2O_3)$ , kaersutite ( $Al_2O_3$ ), Zn ( $ZnO$ ), NiO (NiO), magnetite (FeO), rhodonite (MnO) and kaersutite (MgO).

### **Raman spectrum**

Raman spectrum was procced at the State Key Laboratory of Nuclear Resource and Environment, East China University of Technology. The thin sections were used to perform the Raman spectroscopy analysis by using a Renishaw InVia Raman Spectrometer. A 532 nm laser with spot size of 1–2  $\mu m^2$  was targeted the minerals in the rock sections, where the mineral grains are much large than laser spot size. Each run keeps at least 5 seconds acquisitions. At least 10 same minerals were analysis to confirm its stable Raman spectrum property.

### **In-situ X-Ray Diffraction (In-situ XRD)**

In-situ XRD analysis was performed at Analytic & Testing Research Center of Yunnan by using an X-ray diffractometer (model: Empyrean > D / Max 2200), equipped with a double cross micro region system ( $0.25 \times 0.25 \text{ mm}^2$ ) with laser locator, and Pixel 3D Focus diffractometer ( $265 \times 265$  dot matrix) with a Cu anode X-ray generator ( $K_{\alpha 1}=1.54056 \text{ \AA}$  and  $K_{\alpha 2}=1.54439 \text{ \AA}$ ; Wang et al. 2019). Thin sections of samples are analyzed to obtain the XRD patterns at the diffraction angle ( $2\theta$ ) ranging from  $5^\circ$  to  $90^\circ$  with a step size of  $0.02^\circ$  and the beam spot is  $1 \text{ mm}^2$ . Silicon powder (purity > 99.99%) was used as the reference

to correct the X-ray diffractometer. The cell parameters are refined by MDI Jade 6, which is accurate to the thousandth (Gu et al., 2015).

### **Backscatter electron and energy dispersive spectrometer**

Backscatter electron (BSE) microscopic analysis was performed at the State Key Laboratory of Nuclear Resource and Environment, East China University of Technology by using a scanning electron microscope (FE-SEM, model: Zeiss Gemini Sigma 300 VP SEM), equipped with Oxford Link ISIS energy dispersive spectrometer (EDS) at an operating voltage of 15 kV. The samples were prepared by cutting and polishing into 70  $\mu\text{m}$  sample sections. The coat a layer of carbon film with thickness of 500  $\text{\AA}$  on the surface of sample sections by using the vacuum carbon sprayer. The BSE images are captured by the backscatter electron microscopic detecting instrument. The geochemical mappings of minerals were got by the energy dispersive spectrometer. C, O, Na, Mg, Al, Si, P, S, Cl, K, Ca, Ti, V, Cr, Mn, Fe, Co, Ni, Cu, Zn, As, Pb, Cd, Ba, In and Sn were obtained in this research.

### **TESCAN Integrated Mineral Analysis (TIMA)**

The samples were scanned using TESCAN Integrated Mineral Analysis (TIMA) liberation analysis module equipped at Guangzhou Tuoyan Analytical Technology Co., Ltd. The mineral compositional mappings were obtained on carbon-coated thin sections (mounts) using a MIRA 3 scanning electron microscope. During the analysis, an acceleration voltage of 25 kV and probe current of 8.24 nA were used. Working distance

was set to 15 mm. Pixel spacing was set to 1.5  $\mu\text{m}$  and dot spacing was set to 4.5  $\mu\text{m}$ . The analysis and BSE signal intensity were calibrated on a platinum Faraday cup using the automated procedure. EDS performance was checked by using manganese standard.

### **Whole-rock geochemistry**

The whole-rock geochemistry was performed using inductively coupled plasma optical emission spectrometer (ICP-OES) (Agilent 720) with dilute factor of 1000 at Guangzhou Tuoyan Analytical Technology Co., Ltd. Before analysis, samples were powdered into 200 mesh. The preparation procedures for major elements (except  $\text{SiO}_2$ ) and trace elements are same. The technique of alkali fusion was used to dissolve the samples to analyze  $\text{SiO}_2$ . 0.05 g sample was dissolved with 0.25 g NaOH at 700  $^\circ\text{C}$  in Ag crucible for about 30 minutes and then cool down. Then the samples were dissolved by hot water and acidified by 5 ml HCl and make up to 250 ml for analyzing by ICP-OES. 1g of sample was used to measure the loss on ignition (LOI), including the following steps: 1) samples were weighed in porcelain crucible and heated at 900 $^\circ\text{C}$  in a muffle furnace for 1 h; 2) confirm the LOI by calculating the weighted difference between the untreated sample and residue. The analytical accuracy is less than 2% (relative) for major oxides present in concentrations greater than 0.5 wt% and 5% (relative) for minor oxides present in concentrations between 0.1 wt% and 0.5 wt%. The trace elements were determined by a Jena Plasma Quant inductively-coupled plasma mass spectrometry (ICP-MS). About 0.0500 grams of powdered sample were placed in a Poly tetra fluoro ethylene bomb, and 0.6 ml of HF and

3 ml of HNO<sub>3</sub> were added. The sealed bombs were then placed in an electric oven and heated to 185°C for about 36 h. After cooling, the bombs were heated on a hot plate to evaporate to dryness. 200 ng of Rh was added as an internal standard, and then 2 ml of HNO<sub>3</sub> and 4 ml of water were added. The bombs were again sealed and placed in an electric oven at 135 °C for about 5 hours to dissolve the residue. After cooling, the final dilute factor is about 3000 for ICP-MS analysis.

## RESULTS

### EPMA

The locations of analysis spots are shown in figure 5. Based on the EPMA results shown in attachment 1, a significant V-hosting mineral is recognized. This mineral is extremely rich in vanadium with an average content of 18.62 wt% (V<sub>2</sub>O<sub>3</sub>) (17.55 wt%–19.56 wt%). It also enriches barium with an average of 18.49 wt% (BaO) (17.85 wt%–18.80 wt%) and titanium with an average of 58.81 wt% (TiO) (56.86 wt%–59.72 wt %). Besides, this mineral contents various Cr<sub>2</sub>O<sub>3</sub> (average of 0.67wt%, ranging from 0.52 wt% to 0.84 wt%), SiO<sub>2</sub> (average of 0.34 wt%, ranging from 0.03 wt% to 1.68 wt%) and FeO (average of 0.14 wt%, ranging from 0.02 wt% to 0.86 wt%).

The formula of this mineral is calculated by using the cationic method, and the general steps include: 1) check and correct the average total composition to 100%; 2) calculate the mole quantity of the cations and oxygen atom based on the relative atomic mass and relative content of each part; 3) get the quantity of total cations and oxygen atom; 4)

translate the total cations to theoretical value 9 and get the translate coefficient (Scott and Peatfield 1986; Szymanski 1986), by which the number of cations atom per formula is calculated; 5) set the oxygen atom number to 32, and check the chemical valence equilibrium (Li et al. 2008). The calculated parameters are shown in table 1.

The formula of this V-hosting mineral is obtained as  $[\text{Ba}^{2+}_{0.96} (\text{Ti}^{4+}_{5.87} \text{V}^{3+}_{1.98} \text{Si}^{4+}_{0.07} \text{Cr}^{3+}_{0.07} \text{Fe}^{2+}_{0.02})] \text{O}_{16.00}$ . However, the sum of cations electrovalence in this formula is less than 32 ( $\text{O}_{16}^{32-}$ ). In the hollandite supergroup, only V and Fe exhibit various valences. Hence, the iron atom in this mineral should be  $\text{Fe}^{3+}$ , and the vanadium atom occur as  $\text{V}^{3+}$  and  $\text{V}^{4+}$ . The crystallochemistry formula is recalculated as  $\text{Ba}_{0.96} (\text{Ti}_{5.87} \text{V}^{3+}_{1.87} \text{V}^{4+}_{0.11} \text{Si}_{0.07} \text{Cr}_{0.07} \text{Fe}^{3+}_{0.02}) \text{O}_{16.00}$ , which corresponds to the ideal formula of mannardite ( $\text{BaTi}_6\text{V}_2\text{O}_{16}$ ) (Scott and Peatfield 1986; Szymanski 1986). As a member of hollandite supergroup, mannardite is a hydrated mineral with zeolitic water (about 2.24 wt%  $\text{H}_2\text{O}$ ) (Szymanski 1986; Biagioni et al. 2013; Reznitsky et al. 2018). The average total composition by EPMA (97.20%) (Attachment 1) suggests that the mannardite in this research should be  $[\text{Ba}_{0.96} \cdot \text{H}_2\text{O}] (\text{Ti}_{5.87} \text{V}^{3+}_{1.87} \text{V}^{4+}_{0.11} \text{Si}_{0.07} \text{Cr}_{0.07} \text{Fe}^{3+}_{0.02}) \text{O}_{16.00}$ .

In addition, the crystallochemical formulas of other major minerals in figure 5 are calculated by using cationic method, including pyrite ( $\text{Fe}[\text{S}_2]$ ), quartz ( $\text{SiO}_2$ ), illite ( $(\text{K}_{0.69}, \text{Mg}_{0.17}, \text{Na}_{0.04}) (\text{Al}_{1.61}, \text{Ti}_{0.02}, \text{V}_{0.01}, \text{Fe}_{0.12}) [\text{Al}_{0.85} \text{Si}_{3.15} \text{O}_{10.00}] (\text{OH}, \text{O})$ ), and phengite ( $(\text{K}_{0.41}, \text{Ba}_{0.01}, \text{Na}_{0.01}) [\text{Al}_{1.12} (\text{Al}_{0.08} \text{Si}_{3.92}) \text{O}_{10.00}] (\text{OH})_2$ ). The detail calculated parameters are shown in table 1.

## Raman spectrum

To confirm the crystal structure of the V-hosting mineral, Raman spectrum is proceeded and shows multiple peaks to reflect this V-hosting mineral. The feature of Raman spectrum is in accordance well with the mannardite (Fig. 6). The major peaks at  $133\text{ cm}^{-1}$ ,  $250\text{ cm}^{-1}$ ,  $599\text{ cm}^{-1}$  and  $639\text{ cm}^{-1}$  are assigned to the Ti-O bond (Glass and Fries 2008; Frezzotti et al. 2012). The peak at  $337\text{ cm}^{-1}$  may be assigned to the  $V^{3+}$ -O bond (Reznitskii et al. 1995). The weak peak at around  $1600\text{ cm}^{-1}$  ( $1588\text{ cm}^{-1}$ ) is regard as O-H bond in the  $H_2O$ , which may be affected by the bonds  $Ba^{2+}$ - $H_2O$  (Carey and Korenowski 1998). The weak peak at  $1329$  is assigned to the organic carbon in the shale, which is not the bond of this V-hosting mineral (Beyssac et al. 2002). This Raman spectrum feature further confirms that the V-hosting mineral in the figures 5a–b is mannardite.

## In-situ XRD

The representative XRD patterns for the V-hosting mineral are shown in figure 7. The XRD patterns show the major lattice planes of the V-hosting mineral ((400), (312), (620), (260), (332), (460), (800), (660)), which possesses the same interplanar spacing with mannardite (Fig. 7; Table 2). Besides, the cell parameters are refined by correcting to the thousandth and listed in the table 3. The cell parameters of two analysis spots for SHSD11 are  $a = b = 14.326(1)\text{ \AA}$ ,  $c = 5.887(6)\text{ \AA}$ ,  $V = 1208.37(0)\text{ \AA}^3$  and  $a = b = 14.331(9)\text{ \AA}$ ,  $c = 5.903(6)\text{ \AA}$ ,  $V = 1212.63(0)\text{ \AA}^3$ ; The cell parameters of two analysis spots for SHSD15 are  $a = b = 14.363(8)\text{ \AA}$ ,  $c = 5.902(6)\text{ \AA}$ ,  $V = 1217.83(0)\text{ \AA}^3$  and  $a = b = 14.365(0)\text{ \AA}$ ,  $c =$

5.902(6) Å,  $V = 1218.04(0) \text{ \AA}^3$ . These cell parameters of the V-hosting mineral in this research are exactly similar to mannardite ( $a = b = 14.356(4) \text{ \AA}$ ,  $c = 5.911(3) \text{ \AA}$ ; Scott and Peatfield 1986) with small differences. The differences of cell parameters mainly result from the trace elements in mannardite crystal structure, such as  $\text{Si}^{4+}$  (0.39 Å),  $\text{Fe}^{3+}$  (0.67 Å),  $\text{Cr}^{3+}$  (0.64 Å) and  $\text{V}^{4+}$  (0.59 Å), which has different atom radius from the  $\text{V}^{3+}$  (0.65 Å) (Reznitsky et al. 2018; Zhang and Gao 2012).

### **BSE-EDS**

The BSE-EDS analysis results show detail morphological features for mannardite. As significant carrier of vanadium, the ethmoid and forky branches mannardite exists uniformly in the black shale, minor mannardite exist as vein (Figs. 8a–c, 8g–k), the EDS mapping results suggest that mannardite content extremely high V, Ti and Ba (Figs. 8 d–f).

The micro pyrite, clay minerals and organic carbon were recognized. The pyrite in the black shale is strawberry pyrite (Fig. 5c) and oval nodule pyrite (Figs. 4d and 8g). Clay minerals include illite, mica and kaolinite (Fig. 5d). Organic carbon is filled in the micro interspace of black shale (Fig. 5d).

### **TIMA**

The results of TIMA are shown in table 4. The black carbon siliceous shale (sample SHSD15) consists of mannardite (0.46 vol%), illite (6.60 vol%), quartz (49.67 vol%), albite (12.08 vol%), carbon (29.49 vol%), pyrite (1.15 vol%), and accessory minerals, including apatite, monazite, kaolinite and zircon. The black carbonaceous shale (sample

ZK801D40) consists of mannardite (0.59 vol%), illite (44.82 vol%), carbon (39.22 vol%), quartz (9.44 vol%), pyrite (4.41 vol%), albite (0.94 vol%), and accessory minerals, including actinolite, apatite, monazite and kaolinite.

### **Whole-rock geochemistry**

Total 13 ore samples are analyzed, and the results of whole-rock geochemistry are shown in table 5. The ores hosted in the carbonaceous shales have relatively higher grade of vanadium with average content of 0.83 wt%, ranging from 0.51 wt% to 1.22 wt%. The vanadium in the carbon siliceous shale ranges from 0.36 wt% to 0.95% with average content of 0.60 wt%. The black shale in these vanadium deposits is characterized by high content of Ba with an average of 12030 ppm (2034–24801 ppm) in black carbonaceous shale and 7708 ppm (1670–18344 ppm) in black carbon siliceous shale.

## **DISCUSSION**

### **Occurrence mode of vanadium in mannardite**

Based on the charge balance and EPMA results, the formula of the V-hosting mineral is calculated by cationic method,  $[\text{Ba}_{0.96} \cdot \text{H}_2\text{O}] (\text{Ti}_{5.87} \text{V}^{3+}_{1.87} \text{V}^{4+}_{0.11} \text{Si}_{0.07} \text{Cr}_{0.07} \text{Fe}^{3+}_{0.02}) \text{O}_{16.00}$ , which is consistent with the formula of mannardite ( $\text{BaTi}_6\text{V}_2\text{O}_{16}$ ; Scott and Peatfield 1986; Szymanski 1986). Raman spectrum indicates that the V-hosting mineral contains the  $\text{Ti}^{4+}$ -O ( $133 \text{ cm}^{-1}$ ,  $250 \text{ cm}^{-1}$ ,  $599 \text{ cm}^{-1}$  and  $639 \text{ cm}^{-1}$ ; Glass and Fries 2008; Frezzotti et al. 2012),  $\text{V}^{3+}$ -O bond ( $337 \text{ cm}^{-1}$ ; Reznitskii et al. 1995), O-H bond in  $\text{H}_2\text{O}$  ( $1588 \text{ cm}^{-1}$ ; Carey and Korenowski 1998). From the in-situ XRD patterns, the cell parameters are calculated with

average value of  $a = b = 14.346(7) \text{ \AA}$ ,  $c = 5.899(1)$ ,  $\alpha = \beta = \gamma = 90^\circ$ ,  $Z = 4$ , space group  $I4_1/a$ , which is same with the cell parameters of confirmed mannardite ( $a = b = 14.356(4) \text{ \AA}$ ,  $c = 5.911(3) \text{ \AA}$ ,  $\alpha = \beta = \gamma = 90^\circ$ ,  $Z = 4$ , space group  $I4_1/a$ ; Scott and Peatfield 1986). Combining with the EPMA, Raman spectrum and crystal cell parameters, the V-hosting mineral in this research is mannardite, and the crystal structure model is built (Fig. 9). The mannardite is similar to the ankangite on the chemical composition ( $\text{Ba}_{1.087} \text{Ti}_{5.482} \text{V}_{2.412} \text{Cr}_{0.222} \text{O}_{16.00}$ ) and the two minerals belong to the tetragonal system, which was first reported by Xiong (1986). But there are distinct differences between the two minerals: 1) the mannardite is hydroite, but the ankangite is anhydrous mineral; 2) the cell parameters of mannardite ( $a = b = 14.346(7) \text{ \AA}$ ,  $c = 5.899(1)$ ,  $Z = 4$ , space group  $I4_1/a$ ) is different from the ankangite ( $a = b = 10.118(1) \text{ \AA}$ ,  $c = 2.956(3) \text{ \AA}$ ,  $Z = 1$ , space group  $I4/m$ ; Xiong 1986; Shi et al. 1991).

The trivalent vanadium atom occupies fixed lattice position, forming stable electrovalent bonds ( $\text{V}_2\text{O}_3$ ) (Fig. 9), suggesting that as significant carrier of vanadium in the black shale, mannardite is a vanadium mineral enriching fixed content of vanadium. Different from trivalent vanadium, the minor quadrivalent vanadium enriched in mannardite by replace titanium ( $\text{T}^{4+}$ ) by isomorphism (Fig. 9a), which can be proved by binary isomorphic series of oxyvanite ( $\text{V}_2^{3+}\text{V}^{4+}\text{O}_5$ )-berdesinskiite ( $\text{V}_2^{3+}\text{TiO}_5$ ) with a broad  $\text{V}^{4+}$ - $\text{Ti}^{4+}$  isomorphism (Reznitsky et al. 2018). In the mannardite, various contents of chromium ( $\text{Cr}^{3+}$ ) are detected. Szymanski (1986) found that the chromium atom shares two

fixed positions, occupancies and thermal parameters, which is same with the trivalent vanadium ( $V^{3+}$ ) (Fig. 9a). This suggests that minor trivalent vanadium atoms ( $V^{3+}$ ) (0.65 Å) can be replaced by chromium ( $Cr^{3+}$ ) (0.64 Å), which has similar ionic radius (Zhang and Gao 2012). In this way, the other minor elements (Fe, Si and Al) may replace barium, titanite or vanadium atoms through isomorphism, resulting in slight content variation of vanadium.

### **Contribution of mannardite**

The TIMA results suggest the  $TiO_2$  in the ore mainly derives from mannardite (Fig. 10). Hence, the contents of titanium and vanadium from mannardite have a fixed ratio ( $m(TiO_2) / m(V_2O_5) = 2.60$ ), which can be calculated from the crystallochemical formula of mannardite in this research. The proportion of  $V_2O_5$  in mannardite can be obtained based on the chemical composition of ore rocks, and the detail steps are shown in table 6. The average vanadium provided by mannardite in the ore is 24.95%, ranging from 12.32% to 44.06% (Table 6). This result can be verified by another calculation method using the density and composition of minerals, the steps and results are shown in table 7.

Mannardite contributes 20.98% (SHSD15) and 51.71% (ZK801D40) vanadium in the carbon siliceous shale-hosted ore and carbonaceous shale-host ore, respectively. These results are consistent with the results (19.51% for SHSD15, 44.06% for ZK801D40 in table 6) calculated with the former method. This suggests that as a main hosting mineral, mannardite provides significant vanadium (average of 24.95%) in the black shale-hosted

vanadium deposit.

On the other hand, the vanadium provided by pyrite (0.20%–1.46%) and quartz (3.81%–1.38%) in the black shale is insignificant (Table 7). Especially, as a major clay mineral, illite in the black shale only provides 0.41%–5.34% vanadium (Table 7). Besides, the rest of vanadium probably is enriched in organic compounds by tetraphenyl porphyrin and  $V_2O_4$  (Maylotte et al. 1981; Glikson et al. 1985). This is contradicted with the previous viewpoint that the clay minerals are the major carrier of vanadium in the black shale-hosted vanadium deposits (e. g. Zhang et al. 2015; Zhu et al. 2018).

### **Precipitation mechanism of mannardite**

The previous work on sedimentary environment, sedimentary facies, detrital mineral provenance and isotopes (e.g. S and Pb) have suggested that the vanadium in the black shale mainly derives from pale seawater or surface water (e.g. Evans et al. 1958; Breit and Wanty 1991; Wanty and Goldhaber 1992; Peacock et al. 2004; Ouyang et al. 2010; Wen et al. 2021). Whitmore et al. (2019) confirmed that pentavalent vanadium ( $V^{5+}$ ) is mainly dissolved in the seawater, and the dissolved V in Pacific-derived basin waters was depleted by approximately 15–30% from the effective Pacific Ocean endmember, which accumulated in the sediments by the absorption of Fe oxides particles and uptake of organism. The seawater probably provided considerable vanadium for the precipitation of mannardite in the black shale.

As bioelement, vanadium is controlled significantly by the organism action (Maylotte et

al. 1981; Wanty et al. 1992; Wanty and Goldhaber 1992; Wang and Wilhelmy 2009; Whitmore et al. 2019), which controls the precipitation process of mannardite. As an important organism, the appearance of the algae and plankton during Early Cambrian bio-radiation promoted the accumulation of vanadium by adsorbing vanadium as their parts of lifecycle or by excreting the organic matter to bind vanadium (Brumsack 1983; Lee et al. 1983; Glikson et al. 1985). As a result, vanadium is exceeding rich in the remains of these organism (Fig. 10). Besides, the ferric and aluminum oxides mineral particulates play a significant role in the transportation and accumulation of vanadium before the mannardite precipitation (Breit and Wanty 1991; Whitmore et al. 2019). Shiller and Boyle (1987) found that 40% vanadium are transported by being adsorbed on the surface of these mineral particles, and results from EXAFS spectroscopy further proved that ferric and aluminum oxides particles can adsorb considerable pentavalent vanadium species ( $V^{5+}$ ) (Peacock and Sherman 2004). As multivalent elements, the accumulation of vanadium is affected by the changes of geochemistry condition, especially the reduction reaction associated with organic matter and  $H_2S$  (Mercer et al. 1992; Wanty et al. 1992; Wang and Wilhelmy 2009; Zhang et al. 2015). On the oxidation condition, most vanadium tends to be dissolved in the seawater as pentavalent vanadium species, such as  $H_2VO_4^-$ ,  $H_3VO_4$ ,  $H_4VO_4^+$ ,  $VO_4^{3-}$  (Wanty et al. 1992). The pentavalent vanadium can be reduced into quadrivalent vanadium species by organic matter, and occur as vanadium-organic complexes, such as  $VOOHC_2O_4^-$ ,  $VO(C_2O_4)_2^{2-}$  (Szalay and Szilagyí 1967; Goodman and Cheshire 1975; Perrin 1979; Wilson

and Weber 1979; Wehrli 1987; Wanty et al. 1992).

Furthermore, the following evidences also suggest that the organic matter in the water and sediments contributed significantly on the accumulation and valent changing of vanadium in the precipitation process of mannardite: 1) the passive relation between the vanadium and organic matter in the black shale (Breit and Wanty 1991; Gäbler et al. 2009; Wang and Wilhelmy 2009); 2) the existence of vanadium tetrahedrally coordinated compounds ( $\text{NH}_4\text{VO}_3$ ), short vanadyl bond  $\text{V}_2\text{O}_4$  and octahedrally coordinated compounds ( $\text{V}_2\text{O}_3$ ) in the organic matter detected by X-ray absorption spectroscopy analysis (Maylotte et al. 1981). Besides, various types of pyrite are widespread in the black shale-hosted vanadium deposit, suggesting that the black shale is rich in reduced sulfur species (Patterson et al. 1986). Lots of studies suggested that  $\text{H}_2\text{S}$  in the shale can convert pentavalent vanadium species into quadrivalent vanadium species, and furtherly into trivalent vanadium species, such as  $\text{V}^{3+}$ ,  $\text{VOH}^{2+}$  and  $\text{V}(\text{OH})_2^+$  (Lewan 1984; Tissot and Welte 1984; Breit and Wanty 1991; Peacock and Sherman 2004; Wu et al. 2015; Liu et al. 2017). Hence, as strong reductant, reduced sulfur species prompt vanadium to accumulate in the mannardite. Commonly, the black shale is characterized by high barium (Ba) content (Brumsack 2006; Deng et al. 2019; Charbonnier et al. 2022). In the two vanadium deposits, the black carbonaceous shale contains an average of 12030 ppm Ba, and the black carbon siliceous shale contains an average of 7708 ppm Ba (Table 5), which is distinct higher than the Ba in the Crust (1070 ppm; Shaw et al. 1967). The Ba accumulated in the black shale

mainly exists as bio-barite, a microgranular barite related to the biological process, which is the major form of Ba from the seawater (James 1988; Lu et al. 2004; Griffith et al. 2018). The morphological evidence, nonmetals isotopes, the positive correlation between organic carbon ( $C_{org}$ ) and  $Ba^{2+}$  indicate that Ba in the black shale accumulated mainly by the absorption of plankton plants, and the bio-barite precipitated when the remains of the microorganism degraded (Dymond et al. 1992; Bertram and Cowen 1997; Lu et al. 2004). The abundant biogenic barium (bio-barite) in the black shale further suggests that the accumulation of vanadium is closed related to the organism lifecycle in the water. As major element in the black shale, titanium mainly derives from the detrital minerals (Liu et al. 2019b). Thus, the necessary vanadium, biogenic barium and titanium promote the precipitation of mannardite under a strong reduced condition (Fig. 11). Most of the mannardite precipitates as graininess (Figs. 5a and d) during the diagenesis of the black shale. Meanwhile, part of mannardite was reformed into vein by the late minor hydrothermal process (Figs. 5b and 8g–h), which can be proved by the carbonate vein in the black shale (Fig. 4f).

## IMPLICATIONS

As the key to understanding the accumulation of vanadium in the black shale-hosted deposits, the occurrence mode remains controversial. The recognition of mannardite in the black shale indicates that considerable vanadium occurs as vanadium mineral, and this is significant in terms of metallogenic mechanism of black shale-hosted vanadium deposit.

Based on the precipitation process of mannardite and accumulation features of vanadium in mannardite, vanadium-organic complexes, clay minerals and other minerals, the metallogenic mechanism of black shale-hosted vanadium deposit can be described as following process (Fig. 11): 1) vanadium dissolved in seawater as pentavalent vanadium species on the oxic condition; 2) the initial accumulation of pentavalent vanadium is prompted by the Early Cambrian organism activities and adsorption of Fe, Al oxides mineral particles; 3) the pentavalent vanadium is reduced into quadrivalent species by organic matter on the anoxic condition, and vanadium accumulates furtherly by the complexation and adsorption; 4) the quadrivalent vanadium is reduced into trivalent species by H<sub>2</sub>S under an euxinic condition, which mainly accumulates in mannardite, vanadium-organic complexes and minor comes into clay minerals and other auxiliary minerals by isomorphism in the black shale. Besides, the transformation of vanadium from seawater to sediments and the geochemical composition of mannardite (e. g. V<sup>3+</sup>, Ba, Ti) suggest that the enough biogenic barium (bio-barite), titanium, organic matter, H<sub>2</sub>S (strong reduced condition) are significant factors for the precipitation of mannardite, which are the essential factors for the accumulation of vanadium in the black shale. Based on this essential condition, the Guanyintang, Yangliugang formations and the upper part of Hetang Formation are barren in vanadium mainly due to the following reasons: 1) the impulse supply of vanadium or barium from the seawater; 2) the lack of H<sub>2</sub>S stops the quadrivalent vanadium species from being reduced into trivalent vanadium species.

Previous works suggest that the vanadium in black shale-hosted deposit accumulates mainly as trace metal in clay minerals and organic matter. The vanadium in the two types of minerals was separated by calcining and sulfuric acid leaching (Moskalyk 2003; Niu and Liu 2016; Zeng et al. 2020; Xue et al. 2021b). However, these processes pollute the environment and are ineffective. The mannardite is characterized by large density, 4.28 g/cm<sup>3</sup> (<https://ruff.info/ima/>), which makes it possible to separate the vanadium from the black shale by flotation and the hydrometallurgy (Lu et al. 2012; Feng et al. 2021). Except for the two deposits, the Lower Cambrian vanadium-rich black shale from the South Craton (Fig. 1a) is consistently formed at marine environment and is characterized by high level of Ba (barite) (1548–11404 ppm, even up to 87370 ppm) and organic matter (> 3 wt% and containing H<sub>2</sub>S) (Zhang et al. 1995; Li and Zhang 2009; Chen et al. 2011; Xue et al. 2021a; Xu et al. 2022), which is necessary for the precipitation of mannardite. Hence, the mannardite is probably ubiquitous in the black shale-hosted vanadium deposits at the South China Craton. Based on the proportion of vanadium from the mannardite in this research (average of 24.95%), mannardite in the black shale-hosted vanadium deposits preserve significant vanadium resource in the world (approximately 19.6%), which will increase significantly the beneficiation efficiency and avoid the waste of vanadium resource.

### **ACKNOWLEDGEMENTS**

This research is jointly supported by the Natural Science Fund (Number: H202200072),

the National Natural Science Foundation of China (Number: 92162101), Open Fund Projects of the Key Laboratory of Mass Spectrometry and Instrumentation (Number: JXMS202113) and the Natural Science Fund of East China University of Technology (Number: DHBK2019059). The authors thank the team members from the East China of Technology and the Tenth Geological Brigade of Jiangxi Geological Bureau for their field support, constructive discussions, and comments. Thank the team members of the state Key Laboratory of Nuclear Resources and Environment in East China University of Technology for their help with the EPMA, Raman spectrum, BSE and EDS analysis, the team members of the Analytic & Testing Research Center of Yunnan for the help with in-situ XRD analysis, the team members of Guangzhou Tuoyan Analytical Technology Co., Ltd for help with whole-rock geochemistry and TIMA analysis.

#### REFERENCES CITED

- American Mineralogist Crystal Structure Database, available: <https://rruff.info/> mannardite / R060966.
- Bai, Z.J., Zhong, H., Hu, R.Z., and Zhu, W.G. (2021) World-class Fe-Ti-V oxide deposits formed in feeder conduits by removing cotectic silicates. *Economic Geology*, 116, 681–691.
- Beysac, O., Goffé, B., Chopin, C., Rouzaud, J.N. (2002) Raman spectra of carbonaceous material in metasediments: a new geothermometer. *Journal of Metamorphic Geology*, 20, 859–871.

- Biagioni, C., Capalbo, C., and Pasero, M. (2013) Nomenclature tunings in the hollandite supergroup. *European Journal of Mineralogy*, 25, 85–90.
- Boni, M., Terracciano, R., Evans, N.J., Laukamp, C., Schneider, J., and Bechstädt, T. (2007) Genesis of vanadium ores in the otavi mountainland, Namibia. *Economic Geology*, 102, 441–469.
- Breit, G.N., and Wanty, R.B. (1991) Vanadium accumulation in carbonaceous rocks: A review of geochemical controls during deposition and diagenesis. *Chemical Geology*, 91, 83–97.
- Brumsack, H.J., and Gieskes, J.M. (1983) Interstitial water trace-metal chemistry, of laminated sediments from the Gulf of California, Mexico. *Marine Chemistry*, 14: 89–106.
- Cai, X.F. and Gu, Y.S. (2002) Composite stratigraphic division of the Mesoproterozoic Shuangqiaoshan Group in northern Jiangxi. *Sedimentary Geology and Tethyan Geology*, 22, 79–83 (In Chinese with English abstract).
- Cao, J., Wang, X., and Tao, J. (2019) Petrogenesis of the Piqiang mafic–ultramafic layered intrusion and associated Fe-Ti-V oxide deposit in Tarim Large Igneous Province, NW China. *International Geology Review*, 61, 2249–2275.
- Carey, D.M., and Korenowski, G.M. (1998) Measurement of the Raman spectrum of liquid water. *The Journal of Chemical Physics*, 108, 2669–2675.
- Chen, G.C., Zhang, Q.S., Kong, W.N., Ren, J.G., Peng, J.Y., and Zhang, Y.F. (2011)

- Mineral characteristics and exploration prospect of vanadium deposit of Lower Cambrian black rock series in south Qinling east segment. *Northwestern Geology*, 44, 50–57 (In Chinese with English abstract).
- Chen, J.F., Foland, K.A., Xing, F.M., Xiang, X., and Zhou, T.X. (1991) Magmatism along the southeast margin of the Yangtze block: Precambrian collision of the Yangtze and Cathaysia blocks of China. *Geology*, 19, 815–818.
- Cheng, Y.Q. (1994) *Introduction to Regional Geology in China*. 517 p. Geological Publishing House, Beijing (In Chinese).
- Dang, X.E., Wei, X.H., Li, X.B., Ma, H.Z., and Liu, C.P. (2018) *Metallurgy on the Rare Metals—Tungsten, Molybden and Vanadium*. 255 p. Metallurgical Industry Press, Beijing.
- Density data of minerals are from IMA database of mineral properties, available: <https://rruff.info/ima/>.
- EC, 2018. *Report on Critical Raw Materials and the Circular Economy [R]*. European Commission, Brussels.
- Ettler, V., Jarošíková, A., Mihaljevič, M., Kříbek, B., and Nyambe, I. (2020) Vanadium in slags from smelting of African Pb-Zn vanadate ores: Mineralogy, extractability and potential recovery. *Journal for Geochemical Exploration*, 218, 631–639.
- Feng, Q.C., Yang, W.H., Wen, S.M., Wang, H., Zhao, W.J., and Han, G. (2022) Flotation of copper oxide minerals: A review. *International Journal of Mining Science and*

- Technology, 32, 1351–1364 (In Chinese with English abstract).
- Frezzotti, M.L., Tecce, F., Casagli, A. (2012) Raman spectroscopy for fluid inclusion analysis. *Journal of Geochemical Exploration*, 112, 1–20.
- Gäbler, H.E., Glüh, K., Bahr, A., and Utermann, J. (2009) Quantification of vanadium adsorption by German soils. *Journal of Geochemical Exploration*, 103, 37–44.
- Garrels, R.M., Iii, E., Pommer, A.M., and Coleman, R.G. (1956) Detailed mineral and chemical relations in two uranium–vanadium ores. doi: 10.3133 / tei 635.
- Glass, B.P., and Fries, M. (2008) Micro-Raman spectroscopic study of fine-grained, shock-metamorphosed rock fragments from the Australasian microtektite layer. *Meteoritics and Planetary Science*, 43, 1487–1496.
- Glikson, M., Chappell, B.W., Freeman, R.S., and Webber, E. (1985) Trace elements in oil shales, their source and organic association with particular reference to Australian deposits. *Chemical Geology*, 53, 155–174.
- Gol'dberg, I.S., Kaplan, Z.G., and Ponomarev, V.S. (2010) Patterns of vanadium accumulation in petroleum and natural bitumen. *International Geology Review*, 28, 711–720.
- Griffith, E.M., Paytan, A., Wortmann, U.G., Eisenhauer, A., and Scher, H.D. (2018) Combining metal and nonmetal isotopic measurements in barite to identify mode of formation. *Chemical Geology*, 500, 148–158.
- Gu, Y., Zhang, X.J., Lu, S.G., Jiang, D.P., Wu, A.D. (2015) High rate performance of LiF

- modified  $\text{LiFePO}_4/\text{C}$  cathode material. *Solid State Ionics*, 269, 30–36.
- Henderson, E.P., and Hess, F.L. (1933) Corvusite and rilandite, new minerals from the Utah–Colorado carnotite region. *American Mineralogist*, 18, 195–205.
- Howard, J.M., and Owens, D.R. (1995) Minerals of the Wilson Springs vanadium mines. *Rocks & Minerals*, 70, 154–170.
- JGSEI (2017) Regional geological annals of china, Jiangxi volume. 468p. Geological Publishing House, Beijing.
- Kan, T.X., Li, L.M., Chen, M., Liu, H., Zhao, X.L., Jiang, R., and Han, X. (2022) Provenance of the siliciclastic rocks in the Lower Yangtze region: Implications for Paleozoic tectonic switching of the northeastern South China Block. *Journal of Asian Earth Sciences*, 228, 105145.
- Karpov, S.M., Voloshin, A.V., Savchenko, Y.E., Selivanova, E.A., and Polekhovskii, Y.S. (2012) Coulsonite in the pyrrhotite canyon deposit (Kola Peninsula): The first find in Russia. *Doklady Earth Sciences*, 446, 1064–1066.
- Lee, K., (1983) Vanadium in the aquatic ecosystem. In: J.O. Nriagu (Editor), *Aquatic Toxicology*, Vol. 13. Wiley, New York, 155–187.
- Li, H.L., Li, Z.H., Ou Yang, Y.P., Yang, L.F., Deng, Y.G., Jiang, Q.B., Deng, T., Shang, P., Lin, Y.H., and Zeng, H.X. (2022) Application of principal component analysis and spectrum–area fractal model to identify geochemical anomalies associated with vanadium mineralization in northeastern Jiangxi Province, South China. *Geochemistry:*

- Exploration, Environment, Analysis. doi: 10.1144/geochem2021-090
- Li, M., and Zhang, F.X. (2009) Characteristics of the Zhongcun-Yinhua vanadium deposit in black rock series, Shanyang county, Shanxi Province. *Geology In China*, 36, 1099–1109 (In Chinese with English abstract).
- Li, S.R., Xu, H. and Shen, J.F. (2008) *Crystallography and Mineralogy*. 346 p. Geological Publishing House, Beijing (In Chinese).
- Li, X.H., Li, W.X., Li, Q.L., Wang, X.C., Liu, Y., and Yang, Y.H. (2010) Petrogenesis and tectonic significance of the ~850 Ma Gangbian alkaline complex in South China: Evidence from in situ zircon U-Pb dating, Hf-O isotopes and whole-rock geochemistry. *Lithos*, 114, 1–15.
- Li, X.H., Li, Z.X., Ge, W.C., Zhou, H.W., Li, W.X., Liu, Y., and Wingate, M.T.D. (2003a) Neoproterozoic granitoids in South China: crustal melting above a mantle plume at ca. 825 Ma? *Precambrian Research*, 122, 45–83.
- Li, Z.X., Li, X.H., Kinny, P.D., Wang, J., Zhang, S., and Zhou, H. (2003b) Geochronology of Neoproterozoic syn-rift magmatism in the Yangtze Craton, South China and correlations with other continents: evidence for a mantle superplume that broke up Rodinia. *Precambrian Research*, 122, 85–109.
- Li, Z.X., Qin, M.K., Liu, X.Y., Wang, L.Q., Wang, J. and Li, L.L. (2022) Characteristics, genesis and research significances of multi-elements enrichment layer of black rock series. *World Nuclear Geoscience*, 39, 14–26 (In Chinese with English abstract).

- Liu, N.Q., Yin, Z., Shi, Q., Qian, Z.Y., Wan, G.Q. and Huang, J.F. (2011) Analysis on the Mechanism of Tectonic Movement and Its Ore-Controlling Effect in the Pengshan and Jiujiang-Ruichang Areas, Northern Jianxi Province. *Geology And Exploration*, 47, 333–343 (In Chinese with English abstract).
- Liu, W., Li, H., Chen, Z., Feng, Y., Ji, G., Tian, Y. (2019a) Geochemical characteristics and metal enrichment rules of black shales in the Zhuxi vanadium ore field, eastern Guizhou. *Earth Science*, 44, 2978–2994 (In Chinese with English abstract).
- Liu, W., Lu, X.B., Wu, C.M., and Yang, E.L. (2014) Geochemical Characteristics and Depositional Environment of Early Cambrian Cherts of the Black Shale-Hosted Ag-V Deposit in Kuruktag, Xinjiang, West China. *Acta Geologica Sinica (English Edition)*, 88, 260–261.
- Liu, Z.R.R., Zhou, M.F., Williams Jones, A.E., Wang, W., and Gao, J.F. (2019b) Diagenetic mobilization of Ti and formation of brookite/anatase in early Cambrian black shales, South China. *Chemical Geology*, 506, 79–96.
- Lu, K.K., Xue, J.J., Mei, G.J., Tu, Y.J., and Weng, X.Q. (2012) Research on a new united process of flotation and hydrometallurgy for vanadium extraction from a Low-grade vanadium-bearing stone coal. *Mining Research and Development*, 32, 64–74 (In Chinese with English abstract).
- Lu, Z.C., Liu, C.Q., Liu, J.J., and Wu, F.C. (2004) The bio-barite in witherite deposits from Southern Qinling and its significance. *Progress in Natural Science (English Edition)*,

14, 889–895.

Mao, J.W. (2001) Research progress on the black shale-hosted deposits. *Mineral Deposits*, 20, 402–403 (In Chinese).

Maylotte, D.H., Wong, J., Peters, R.L., Lytle, F.W., and Gregor, R.B. (1981) X-ray absorption spectroscopic investigation of trace vanadium sites in coal. *Science*, 214, 554–556.

Mercer, G.E., Fitzgerald, S., Day, J., and Filby, R.H. (1992) Determination of organic/inorganic associations of trace elements in kerogen of the New Albany shale. *Fuel*, 72, 1187–1195.

Micera, G., and Dallochio, R. (1988) Metal complex formation on the surface of amorphous aluminium hydroxide. Part IV. Interaction of oxovanadium(IV) and vanadate(V) with aluminium hydroxide in the presence of succinic, malic and 2-mercaptosuccinic acids. *Colloids and Surfaces*, 34, 185–196.

Moskalyk, R.R., Alfantazi, A.M. (2003). Processing of vanadium: a review. *Minerals Engineering*, 16, 793–805.

Niu, L., and Liu, Z.N. (2016) The study on extraction of  $V_2O_5$  from stone coal with vanadium by combing mineral processing and metallurgy. *Hunan Nonferrous Metals*, 32, 35–38 (In Chinese with English abstract).

Qian, Z.Y. and Wei, Y.H. (2019) Geological characteristics and analysis of sources of ore-bearing rock series of Lijiashan vanadium deposit in Pengze County. *World nonferrous*

metals, 16, 106-161 (In Chinese with English abstract).

- Reznitskii, L.Z., Sklyarov, E.V., Ushchapovskaya, Z. F. (1995) Magnesiocoulsonite  $MgV_2O_4$  — a new mineral species in the spinel group. *Zapiski Vserossijskogo Mineralogicheskogo Obshchestva*, 124, 91–98.
- Reznitsky, L.Z., Sklyarov, E.V., Ushchapovskaya, Z.F., and Barash, I.G. (2018) The First find of mannardite in Russia. *Doklady Earth Sciences*, 479, 397–400.
- Schmid, S., Taylor, W.R., and Jordan, D.P. (2020) The Bigryli tabular sandstone-hosted uranium-vanadium deposit, Ngalia Basin, Central Australia. *Minerals*, 10, 896. doi: 10.3390 / min10100896.
- Schulz, K.J., DeYoung, J.H., Jr., Seal, R.R., II, and Bradley, D.C., Ed. (2017) Critical mineral resources of the United States—Economic and environmental geology and prospects for future supply, 797 p. U.S. Geological Survey, Washington.
- Scott, J.D., and Peatfield, G.R. (1986) Mannardite  $[Ba.H_2O](Ti_6V(\text{super } 3^+)_2)O_{16}$ , a new mineral species, and new data on redledgeite. *The Canadian Mineralogist*, 24, 55–66.
- Sergeeva, N.E., Eremin, N.I., and Dergachev, A.L. (2011) Vanadium mineralization in ore of the vihanti massive sulfide basemetal deposit, Finland. *Geology*, 436, 800–803.
- Shaw, D.M., Reilly, G.A., Muysson, J.R., Pattenden, G.E., Campbell, F.E. (1967) An estimate of the chemical composition of the Canadian Precambrian shield, *Canadian Journal of Earth Sciences*, 4, 829–853.
- Shi, N.C., Ma, Z.S., Liu, W. (1991) Crystal structure determination of Ankangite with one

- dimensional incommensurate modulation. *Acta Petrologica Et Mineralogica*, 10, 233–246 (In Chinese with English abstract).
- Spry, P.G., and Scherbarth, N.L. (2006) The gold-vanadium-tellurium association at the Tuvatu gold-silver prospect, Fiji: conditions of ore deposition. *Mineralogy and Petrology*, 87, 171–186.
- Sracek, O., Mihaljevič, M., Kříbek, B., Majer, V., Filip, J., Vaněk, A., Penížek, V., Ettler, V., and Mapani, B. (2014) Geochemistry and mineralogy of vanadium in mine tailings at Berg Aukas, northeastern Namibia. *Journal of African Earth Sciences*, 96, 180–189.
- Surveying and Mapping Team in Jiangxi (1971) The 1:200,000 Hukou geology map, Nanchang (In Chinese).
- Szymanski, J.T. (1986) The crystal structure of mannardite, a new hydrated cryptomelane–group (hollandite) mineral with a doubled short axis. *Canadian Mineralogist*, 24, 67–78.
- Tang, X., Jiang, Z., Li, Z., Cheng, L., Zhang, Y., Sun, P., and Fan, C. (2017) Factors controlling organic matter enrichment in the Lower Cambrian Niutitang Formation Shale on the eastern shelf margin of the Yangtze Block, China. *Interpretation*, 5, T399–T410.
- USGS (2022), Mineral commodity summaries 2022, 202 p. U.S. Geological Survey, Washington.
- Villanova-de-Benavent, C., Torró, L., Castillo-Oliver, M., Campeny, M., Melgarejo, J.C.,

- Llovet, X., Galí, S., and Gonçalves, A.O. (2017) Fe-Ti(-V) oxide deposits of the Kunene anorthosite complex (SW Angola): Mineralogy and Thermo-Oxybarometry. *Minerals*, 7, 246. doi:10.3390/min7120246.
- Wan, T.F. (2010) *The Tectonics of China: Data, Map and Evolution*. 501 p. Higher Education Press, Beijing.
- Wang, D., and Wilhelmy, S.A.S (2009) Vanadium speciation and cycling in coastal waters. *Marine Chemistry*, 117, 52–58.
- Wang, L., Zhang, Q.P., and Sun, W. (2017) Research on occurrence of vanadium in stone coal deposit at Loufanggou area, Shangluo City, Shanxi Province, China. *Acta Mineralogica Sinica*, 37, 29–35 (In Chinese with English abstract).
- Wang, Q.X. and Ma, H.L. (2009) Status and prospects of V<sub>2</sub>O<sub>5</sub> product research and production and China's vanadium resources. *Conservation And Utilization of Mineral Resources*, 5, 47–50 (In Chinese with English abstract).
- Wang, W., Guan, C.G., Hu, Y.L., Cui, H., Muscente, A.D., Chen, L., and Zhou, C.M. (2020) Spatial and temporal evolution of Ediacaran carbon and sulfur cycles in the Lower Yangtze Block, South China. *Palaeogeography, Palaeoclimatology, Palaeoecology*, 537, 109417.
- Wang, X., Xu X.X., Ye, Y., Wang, C., Liu, D., Shi, X.C., Wang, S., Zhu, X. (2019) In-situ High-Temperature XRD and FTIR for Calcite, Dolomite and Magnesite: Anharmonic Contribution to the Thermodynamic Properties. *Journal of Earth Science*, 30, 964–976.

- Wang, Y., Han, Q., Bo, H., Li, W.C., Wang, H., Wang T.T. and Zhou, S. (2013). Geochemistry and sedimentary environment of Lower Cambrian black rock series in Xiuwu region. *Gansu Geology*, 22, 28–34 (In Chinese with English abstract).
- Wanty, R.B., and Goldhaber, M.B. (1992) Thermodynamics and kinetics of reactions involving vanadium in natural systems: Accumulation of vanadium in sedimentary rocks. *Geochemical Cosmochim Acta*, 56, 1471–1483.
- Whitmore, L.M., Morton, P.L., Twining, B.S., and Shiller, A.M. (2019) Vanadium cycling in the Western Arctic Ocean is influenced by shelf-basin connectivity. *Marine Chemistry*, 216, 103701.
- Wülser, P.A., Brugger, J., Foden, J., and Pfeifer, H.R. (2011) The Sandstone-Hosted Beverley uranium deposit, Lake Frome Basin, South Australia: Mineralogy, Geochemistry, and a time-constrained model for its genesis. *Economic Geology*, 106, 835–867.
- Xiong, M. (1988) A new mineral—ankangite. *Chinese Science Bulletin*, 33, 1401-1404 (In Chinese).
- Xu, L.G., Fu, X.R., Ye, H.S., Zheng, W., Chen, B., and Fang, Z.L. (2022) Geochemical composition and paleoceanic environment of the Lower Cambrian black shale-hosted Qianjiaping vanadium deposit in the southern Qinling Region. *Earth Science Frontiers*, 29, 160–175 (In Chinese with English abstract).
- Xue, N.N., Zhang, Y.M., Liu, T., and Zheng, Q. (2021b) Efficient separation of black shale-

- hosted vanadium induced by formation of kalunite-jarosite solid solution in two stage pressurized acid leaching coupled with lixivium recycling. *Separation and Purification Technology*, 269, 118762.
- Xue, Z.X., Gao, J.B., Yang, R.D., Xu, H., Chen, J., and Gao, L. (2021a) Enrichment mechanism of vanadium in Lower Cambrian black rock series in Sansui, southeastern Guizhou. *Geological Review*, 67, 1321–1331 (In Chinese with English abstract).
- Yang, L.F., Li, Z.H., OuYang, Y.P., Deng, T., Deng, Y.G., Meng, D.L., and Zheng, H. (2022) Research progress and prospect of vanadium deposits. *Sedimentary Geology and Tethyan Geology* (In Chinese with English abstract).
- Yang, M. G., Wu, F.J., Song, Z.R. and Lv, S.J. (2015) North Jiangxi: A geological window of South China. *Acta Geologica Sinica*, 89, 222–233 (In Chinese with English abstract).
- Yang, M.G. (2011) Characteristics and evolution of Qinhang suture zone and Qinhang metallogenic belt. In *Geological Society of Jiangxi Province (2011) Recent advance on Geology of Jiangxi Province*, p. 1–14, Jiangxi Science and Technology Publishing House, Nanchang (In Chinese).
- Yi, Y., Pi, D.H., and Jiang, S.Y. (2017) Occurrence, source and enrichment mechanism of silver in black shale–hosted Baiguoyuan Ag-V ore deposit, Hubei Province, China. *Journal of Geochemical Exploration*, 183, 79–87.
- Zeng, S.Q., Chen, H., Qin, Y., Deng, B., Deng, S.W., and Tian, Z.P. (2020) Experimental

- study on beneficiation and metallurgy of a black shale vanadium ore in Hunan Province. *Mining Research and Development*, 40, 108–112 (In Chinese with English abstract).
- Zhang, H.F., and Gao, S. (2012) *Geochemistry*. 410. p, Geological Publishing House, Beijing (In Chinese).
- Zhang, Q., Dong, C.S., and Zhan, X.Z. (1995) Geochemical characteristics of Baiguoyuan black shale-type Ag-V deposit in western Hubei Province. *Acta Mineralogica Sinica*, 15, 185–191 (In Chinese with English abstract).
- Zhang, Y.B., Zhang, Q., Cai, Y., Wang, D.P., and Li, K.W. (2015) The occurrence state of vanadium in the black shale-hosted vanadium deposits in Shangling of Guangxi Province, China. *Chinese Journal of Geochemistry*, 34, 484–497.
- Zhang, Y.M., Bao, S.X., Liu, T., Chen, T.J., and Huang, J. (2011) The technology of extracting vanadium from stone coal in China: History, current status and future prospects. *Hydrometallurgy*, 109, 116–124.
- Zhao, X.X. (2020) Geological characteristics and genesis of vanadium deposit in Yangjiashan mining area, Pengze County, Jiangxi Province. *Mineral resources*, 21, 82-83 (In Chinese with English abstract).
- Zhou, H.D. (1990) On the mechanism and the characteristics of Early Cambrian "Stone Coal" in Lower Yangtze region and their relation to petroliferous potentials. *Experimental Petroleum Geology*, 12, 36–43 (In Chinese with English abstract).

Zhou, M.F., Chen, W.T., Wang, C.Y., Prevec, S.A., Liu, Patricia P., and Howarth, G.H.

(2013) Two stages of immiscible liquid separation in the formation of Panzhihua-type Fe-Ti-V oxide deposits, SW China. *Geoscience Frontiers*, 4, 481–502.

Zhou, X.J., Li, S.Q. and Wang, G.Y. (2019) Geological characteristics and metallogenic

regularity of vanadium deposits in black rock series in Northern Jiangxi Province. *World Nonferrous Metals*, 22, 183–185 (In Chinese with English abstract).

Zhou, Y.H., Lin, L., Wen, C.Q., Mi, W.T., Zhu, L.D., Zhu, K.Y., Yang, W.G., and Pang, Y.C.

(2020) Study on the occurrence state of Ni-Mo-V from the poly-metallic layers in the Niutitang Formation. *Mineralogy and Petrology*, 40, 67–81 (In Chinese with English abstract).

Zhu, D., Lu, L., Wei, J.Q., Wang, F., Gui, F.Y., and Pan, S.Y. (2018) Study of vanadium in

early Cambrian black shales—A case study of the Tongshan mine, South China. *Resources Environment & Engineering*, 32, 473–480 (In Chinese with English abstract).

## **FIGURE CAPTIONS**

**FIGURE 1.** (a) Tectonic framework of SE China (modified after Cheng 1994) and (b) Geology of Jiujiang Basin showing the location of major vanadium deposits (modified after Surveying and Mapping Team in Jiangxi 1971; JGSEI 2017). The deposits data are from Mao 2001, Liu et al. 2014, Zhang et al. 2015, Yi et al. 2017, Zhu et al. 2018, Zhou et al. 2019, 2020, Li et al. 2022a and Yang et al. 2022.

**FIGURE 2.** (a) Geological map and (b) geological section of Yangjiashan vanadium deposit

**FIGURE 3.** (a) Geological map and (b) geological section of Liujiqiao vanadium deposit

**FIGURE 4.** Geological outcrop and macroscopic features of samples from the black shale-hosted vanadium deposits. (a) Hetang Formation is contact conformably with the overlying Guanyintang Formation. (b) Alternating layers of thick carbonaceous shale and thin carbon siliceous shale of Hetang Formation. (c, e–f) Black shale rich in organic matter from Hengtang Formation. (d) Pyrite nodule-bearing carbon siliceous shale from Hetang Formation.

**FIGURE 5.** Micrographs of mannardite and other minerals showing parts of EPMA analysis spot (yellow dots with size of 1  $\mu\text{m}$ ). (a–b) Mannardite in the black shale. (c) Strawberry pyrite. (d) Organic carbon filled in the interspace of clay minerals and quartz. Ill = illite; Man = mannardite; Py = pyrite; Q = quartz.

**FIGURE 6.** Raman spectrum of the V-Ti-Ba oxide in this research and mannardite. Yellow dots in (b) show parts of the Raman analysis locations. Raman spectrum data of mannardite in (c) are from American Mineralogist Crystal Structure Database, available: <https://ruff.info/mannardite/R060966>.

**FIGURE 7.** In-situ XRD patterns of the V-Ti-Ba oxide in the black shale hosted vanadium deposit. The red spots show some of in-situ XRD analysis locations. The patterns of mannardite (PDF # 42-0615) are from Scott and Peatfield (1986).

**FIGURE 8.** Micrographs of BSE and EDS mapping of mannardite from the black shale.

(a) Ethmoid mannardite; (b) Branches mannardite. (c) Ethmoid mannardite distribute uniformly. (d)–(f) EDS mapping of mannardite in (c) showing V, Ti, Ba content. (i)–(k) EDS mapping of mannardite vein in (h) showing V, Ti, Ba content.

**FIGURE 9.** Crystal structure model of mannardite from the vanadium deposits. Crystal cell parameters are from Szymanski 1986 and Reznitsky et al. 2018.

**FIGURE 10.** Micrographs of BSE and TIMA analysis of vanadium ore hosed in the black shale

**FIGURE 11.** Precipitation process of mannardite and metallogenic mechanism of black shale-hosted vanadium deposits

**TABLE 1.** Average EPMA results and parameters for calculating crystallochemical formula

| Mannardite                     | Content measured<br>(wt %) | Sigma ( $1\sigma$ ) | Content<br>corrected (wt %) | Molecular<br>mass | Mole<br>number | Cation<br>number | Cations<br>per formula |
|--------------------------------|----------------------------|---------------------|-----------------------------|-------------------|----------------|------------------|------------------------|
| TiO <sub>2</sub>               | 58.81                      | 0.80                | 60.47                       | 79.90             | 0.76           | 0.76             | 5.87                   |
| BaO                            | 18.49                      | 0.27                | 19.01                       | 153.33            | 0.12           | 0.12             | 0.96                   |
| Cr <sub>2</sub> O <sub>3</sub> | 0.67                       | 0.09                | 0.69                        | 151.99            | 0.00           | 0.01             | 0.07                   |
| V <sub>2</sub> O <sub>3</sub>  | 18.62                      | 0.49                | 19.14                       | 149.88            | 0.13           | 0.26             | 1.98                   |
| SiO <sub>2</sub>               | 0.53                       | 1.23                | 0.54                        | 60.08             | 0.01           | 0.01             | 0.07                   |
| FeO                            | 0.14                       | 0.17                | 0.14                        | 71.84             | 0.00           | 0.00             | 0.02                   |
| Total                          | 97.26                      |                     | 100.00                      |                   |                |                  |                        |
| Quartz                         |                            |                     |                             |                   |                |                  |                        |
| K <sub>2</sub> O               | 0.05                       |                     | 0.05                        | 94.20             | 0.00           | 0.00             | 0.00                   |
| SiO <sub>2</sub>               | 96.43                      |                     | 99.50                       | 60.08             | 1.66           | 1.66             | 1.00                   |
| Al <sub>2</sub> O <sub>3</sub> | 0.30                       |                     | 0.31                        | 101.96            | 0.00           | 0.01             | 0.00                   |
| FeO                            | 0.09                       |                     | 0.09                        | 71.84             | 0.00           | 0.00             | 0.00                   |
| V <sub>2</sub> O <sub>3</sub>  | 0.05                       |                     | 0.05                        | 149.88            | 0.00           | 0.00             | 0.00                   |
| Total                          | 96.91                      |                     | 100.00                      |                   |                |                  |                        |
| Illite                         |                            |                     |                             |                   |                |                  |                        |
| K <sub>2</sub> O               | 8.07                       |                     | 8.84                        | 94.20             | 0.09           | 0.19             | 0.69                   |

|                                |       |        |        |      |      |      |
|--------------------------------|-------|--------|--------|------|------|------|
| MgO                            | 1.74  | 1.91   | 40.30  | 0.05 | 0.05 | 0.17 |
| Na <sub>2</sub> O              | 0.33  | 0.36   | 61.98  | 0.01 | 0.01 | 0.04 |
| SiO <sub>2</sub>               | 47.23 | 51.74  | 60.08  | 0.86 | 0.86 | 3.15 |
| Al <sub>2</sub> O <sub>3</sub> | 31.35 | 34.34  | 101.96 | 0.34 | 0.67 | 2.46 |
| FeO                            | 2.07  | 2.27   | 71.84  | 0.03 | 0.03 | 0.12 |
| V <sub>2</sub> O <sub>3</sub>  | 0.15  | 0.16   | 149.88 | 0.00 | 0.00 | 0.01 |
| TiO <sub>2</sub>               | 0.36  | 0.39   | 79.87  | 0.00 | 0.00 | 0.02 |
| Total                          | 91.28 | 100.00 |        |      | 1.82 |      |
| Pyrite                         |       |        |        |      |      |      |
| S                              | 52.29 | 53.51  | 32.07  | 1.67 |      |      |
| Mn                             | 0.15  | 0.15   | 54.94  | 0.00 | 0.00 | 0.00 |
| Fe                             | 45.08 | 46.13  | 55.85  | 0.83 | 0.83 | 1.00 |
| As                             | 0.21  | 0.21   | 74.92  | 0.00 |      |      |
| Total                          | 97.73 | 100.00 |        |      | 0.83 |      |
| Phengite                       |       |        |        |      |      |      |
| K <sub>2</sub> O               | 5.86  | 6.13   | 94.20  | 0.07 | 0.13 | 0.41 |
| BaO                            | 0.26  | 0.28   | 153.33 | 0.00 | 0.00 | 0.01 |
| Na <sub>2</sub> O              | 0.05  | 0.05   | 61.98  | 0.00 | 0.00 | 0.01 |

|                                |       |        |        |      |      |      |
|--------------------------------|-------|--------|--------|------|------|------|
| SiO <sub>2</sub>               | 70.87 | 74.10  | 60.08  | 1.23 | 1.23 | 3.92 |
| Al <sub>2</sub> O <sub>3</sub> | 18.50 | 19.35  | 101.96 | 0.19 | 0.38 | 1.20 |
| FeO                            | 0.08  | 0.09   | 71.84  | 0.00 | 0.00 | 0.00 |
| V <sub>2</sub> O <sub>3</sub>  | 0.02  | 0.02   | 149.88 | 0.00 | 0.00 | 0.00 |
| Total                          | 95.64 | 100.00 |        |      | 1.75 |      |

**Note:** In the analysis results of the quartz, illite, pyrite and phengite, the analytical accuracy is less than 1% (relative) for the major oxides (> 5 wt%), less than 5% (relative) for the minor oxides (1–5 wt %) and 5–10% (relative) for the trace oxides (< 1 wt%).

**TABLE 2.** In-situ XRD results of V-hosting mineral in black shale-hosted vanadium deposits

| (hkl) | d(Å)     |          |          |          |            |
|-------|----------|----------|----------|----------|------------|
|       | SHSD11-1 | SHSD11-2 | SHSD15-1 | SHSD15-2 | Mannardite |
| (400) | 3.581(5) | 3.583(0) | 3.583(9) | 3.580(3) | 3.582(0)   |
| (420) | 3.196(1) |          | 3.205(5) | 3.202(3) | 3.204(0)   |
| (240) |          | 3.204(7) |          |          | 3.204(0)   |
| (132) |          |          |          | 2.472(9) | 2.472(0)   |
| (312) | 2.460(0) | 3.473(5) | 2.465(6) |          | 2.472(0)   |
| (620) | 2.260(0) | 2.266(1) | 2.266(6) |          | 2.266(0)   |
| (260) |          |          |          | 2.264(4) | 2.266(0)   |

|       |          |          |          |          |          |
|-------|----------|----------|----------|----------|----------|
| (332) | 2.215(2) | 2.222(8) | 2.217(1) | 2.222(1) | 2.222(0) |
| (460) | 1.982(0) |          | 1.988(0) | 1.986(0) | 1.987(0) |
| (640) |          | 1.987(5) |          |          | 1.987(0) |
| (800) | 1.787(8) | 1.791(5) | 1.791(9) | 1.790(1) | 1.791(0) |
| (660) | 1.688(0) | 1.689(0) | 1.689(5) | 1.687(8) | 1.689(0) |
| (732) | 1.585(1) |          |          |          | 1.586(0) |
| (372) |          | 1.586(8) |          | 1.586(0) | 1.586(0) |
| (572) | 1.449(5) |          | 1.449(5) |          | 1.451(0) |

**Note:** the cell parameters of mannardite are from Scott and Peatfield (1986). The uncertainties of the last digits are presented in the parentheses.

**TABLE 3.** Cell parameters of V-hosting mineral in black shale-hosted vanadium deposits

| Sample     | a(Å)      | a(Å)      | a(Å)     | V(Å <sup>3</sup> ) | $\alpha$ (°) | $\beta$ (°) | $\gamma$ (°) | Z   | Space group                       |
|------------|-----------|-----------|----------|--------------------|--------------|-------------|--------------|-----|-----------------------------------|
| SHSD11-1   | 14.326(2) | 14.326(2) | 5.887(6) | 1208.37(0)         | 90           | 90          | 90           | 4.0 | <i>I4</i> <sub>1</sub> / <i>a</i> |
| SHSD11-2   | 14.331(9) | 14.331(9) | 5.903(6) | 1212.63(0)         | 90           | 90          | 90           | 4.0 | <i>I4</i> <sub>1</sub> / <i>a</i> |
| SHSD15-1   | 14.365(1) | 14.365(1) | 5.902(7) | 1218.04(0)         | 90           | 90          | 90           | 4.0 | <i>I4</i> <sub>1</sub> / <i>a</i> |
| SHSD15-2   | 14.363(9) | 14.363(9) | 5.902(6) | 1217.83(0)         | 90           | 90          | 90           | 4.0 | <i>I4</i> <sub>1</sub> / <i>a</i> |
| Average    | 14.346(7) | 14.346(7) | 5.899(1) | 1214.22(0)         | 90           | 90          | 90           | 4.0 | <i>I4</i> <sub>1</sub> / <i>a</i> |
| Mannardite | 14.356(4) | 14.356(4) | 5.911(3) |                    | 90           | 90          | 90           | 4.0 | <i>I4</i> <sub>1</sub> / <i>a</i> |

**Note:** the cell parameters of mannardite are from Scott and Peatfield (1986). The uncertainties of the last digits are presented in the parentheses.

**TABLE 4.** TIMA analysis results showing the mineral constituent of vanadium ore (vol%)

| Sample   | Illite   | Quartz   | Pyrite  | Albite   | Mannardite | Actinolite | Apatite | Monazite | Kaolinite | Zircon  | Carbon   |
|----------|----------|----------|---------|----------|------------|------------|---------|----------|-----------|---------|----------|
| SHSD15   | 6.60(3)  | 49.67(3) | 1.15(5) | 12.08(2) | 0.45(5)    | --         | 0.45(1) | 0.00(3)  | 0.08(7)   | 0.00(0) | 29.49(0) |
| ZK801D40 | 44.82(3) | 9.44(0)  | 4.40(6) | 0.93(7)  | 0.58(8)    | 0.40(0)    | 0.16(7) | 0.00(7)  | 0.00(6)   | 0.00(0) | 39.22(2) |

**Note:** The uncertainties of the last digits are presented in the parentheses.

**TABLE 5.** Whole-rock geochemistry results of vanadium ore hosted in the black shale (ppm for V and Ba, wt% for the others)

| Sample    | Ore                 | Al <sub>2</sub> O <sub>3</sub> | K <sub>2</sub> O | TiO <sub>2</sub> | Fe <sub>2</sub> O <sub>3</sub> | LOI   | SiO <sub>2</sub> | V    | V <sub>2</sub> O <sub>5</sub> * | Ba    |
|-----------|---------------------|--------------------------------|------------------|------------------|--------------------------------|-------|------------------|------|---------------------------------|-------|
| ZK801 D32 |                     | 10.61                          | 3.15             | 0.46             | 6.17                           | 18.86 | 53.45            | 4520 | 0.81                            | 8073  |
| ZK801 D40 |                     | 10.65                          | 3.42             | 0.58             | 8.14                           | 19.75 | 51.29            | 2840 | 0.51                            | 14353 |
| ZK801 D14 | Ore hosted in black | 10.18                          | 3.12             | 0.56             | 5.26                           | 16.40 | 53.60            | 5010 | 0.89                            | 24801 |
| ZK801 D15 | carbonaceous shale  | 7.87                           | 2.04             | 0.39             | 3.98                           | 19.81 | 54.43            | 6840 | 1.22                            | 10888 |
| ZK801 d21 |                     | 15.30                          | 4.13             | 0.69             | 8.14                           | 17.77 | 50.16            | 3990 | 0.71                            | 2034  |
| Average   |                     | 10.92                          | 3.18             | 0.54             | 6.34                           | 18.52 | 52.59            | 4640 | 0.83                            | 12030 |
| SHS D04   |                     | 5.65                           | 1.41             | 0.33             | 2.51                           | 15.69 | 71.53            | 2550 | 0.46                            | 13424 |

|           |                        |      |      |      |      |       |       |      |      |       |
|-----------|------------------------|------|------|------|------|-------|-------|------|------|-------|
| SHS D11   | Ore hosted in black    | 5.85 | 1.22 | 0.31 | 5.29 | 12.42 | 70.97 | 2310 | 0.41 | 4308  |
| ZK801 D07 | carbon siliceous shale | 5.29 | 1.36 | 0.32 | 2.29 | 15.09 | 70.54 | 2010 | 0.36 | 8271  |
| SHS D15   |                        | 8.91 | 1.94 | 0.48 | 2.55 | 12.46 | 69.67 | 5350 | 0.95 | 5940  |
| SHS D21   |                        | 9.34 | 2.26 | 0.44 | 2.88 | 19.34 | 61.98 | 5030 | 0.90 | 6982  |
| ZK801 D12 |                        | 7.38 | 1.95 | 0.37 | 4.56 | 16.69 | 61.85 | 4930 | 0.88 | 18344 |
| ZK801 D27 |                        | 4.51 | 1.07 | 0.22 | 1.84 | 15.20 | 72.40 | 2140 | 0.38 | 2724  |
| ZK801 D29 |                        | 4.09 | 0.85 | 0.21 | 1.51 | 8.45  | 80.81 | 2550 | 0.46 | 1670  |
| Average   |                        | 6.38 | 1.51 | 0.33 | 2.93 | 14.42 | 69.97 | 3359 | 0.60 | 7708  |

**Note:** V<sub>2</sub>O<sub>5</sub>\* is calculated by content of V (ppm) in the ore. The analytical accuracy is less than 2% (relative) for the major oxides (> 0.5 wt%) and less than 5% (relative) for minor oxides (0.1–0.5 wt%).

**TABLE 6.** Occupancies of vanadium in mannardite calculated by whole-rock geochemical and EPMA results

| Elements  | Total V <sub>2</sub> O <sub>5</sub> in ore (wt%) | TiO <sub>2</sub> in ore (wt%) | V <sub>2</sub> O <sub>5</sub> in mannardite (wt%) (calculated) | Contribution (%) |
|-----------|--|-------------------------------|--|------------------|
| SHS D04   | 0.46   | 0.33                          | 0.13   | 27.85            |
| SHS D11   | 0.41   | 0.31                          | 0.12   | 28.48            |
| ZK801 d07 | 0.36   | 0.32                          | 0.12   | 33.79            |
| SHS D15   | 0.95   | 0.48                          | 0.19   | 19.51            |
| SHS D21   | 0.90   | 0.44                          | 0.17   | 18.93            |

|           |      |      |      |       |
|-----------|------|------|------|-------|
| ZK801 d12 | 0.88 | 0.37 | 0.14 | 16.09 |
| ZK801 d14 | 0.89 | 0.56 | 0.22 | 24.29 |
| ZK801 d15 | 1.22 | 0.39 | 0.15 | 12.32 |
| ZK801 d21 | 0.71 | 0.69 | 0.27 | 37.29 |
| ZK801 d27 | 0.38 | 0.22 | 0.08 | 21.90 |
| ZK801 d29 | 0.46 | 0.21 | 0.08 | 18.12 |
| ZK801 d32 | 0.81 | 0.46 | 0.18 | 21.72 |
| ZK801 d40 | 0.51 | 0.58 | 0.22 | 44.06 |
| Average   | 0.69 | 0.41 | 0.16 | 24.95 |

**Note:** For the total V<sub>2</sub>O<sub>5</sub> and TiO<sub>2</sub> in ore, the analytical accuracy is less than 2% (relative) when the content is greater than 0.5 wt%, and the accuracy is less than 5% (relative) when the content ranges from 0.1 wt% to 0.5 wt%. Steps of calculating proportion of vanadium from mannardite: 1) calculate the mass ratio of TiO<sub>2</sub> and V<sub>2</sub>O<sub>5</sub> in the ore rock by the EPMA results of mannardite,  $m(\text{TiO}_2) / m(\text{V}_2\text{O}_5) = 2.60$ ; 2) obtain the mass ratio of V<sub>2</sub>O<sub>5</sub> from mannardite in the ore rock based on the content of TiO<sub>2</sub>,  $\text{V}_2\text{O}_{5(\text{mannardite})} = m(\text{TiO}_2) / 2.60$ ; 3) get the proportion (P) of V<sub>2</sub>O<sub>5</sub> from mannardite in the ore rock,  $P = m(\text{V}_2\text{O}_{5(\text{mannardite})}) / m(\text{V}_2\text{O}_{5(\text{total})})$ .

**TABLE 7.** Occupancies of vanadium in minerals calculated by whole-rock geochemistry, TIMA and EPMA results (wt%)

| Mineral | V <sub>2</sub> O <sub>5</sub> # | Sigma<br>(1σ) | Density | Volume<br>fraction | SHSD15  |                  |                        | ZK801D40  |                  |  |
|---------|---------------------------------|---------------|---------|--------------------|---|------------------|------------------------|---|------------------|--|
|         |                                 |               |         |                    | with total 0.95 wt% V <sub>2</sub> O <sub>5</sub> |                  |                        | with total 0.51 wt% V <sub>2</sub> O <sub>5</sub> |                  |  |
|         |                                 |               |         |                    | Mass fraction                                     | Occupancy<br>(%) | Volume<br>fraction (%) | Mass fraction<br>(wt%)                            | Occupancy<br>(%) |  |

|            |       |      |      |        |       |       |        |       |       |
|------------|-------|------|------|--------|-------|-------|--------|-------|-------|
| Illite     | 0.05  | 0.01 | 2.70 | 6.60   | 8.07  | 0.41  | 44.82  | 56.08 | 5.34  |
| Quartz     | 0.06  | 0.01 | 2.65 | 49.67  | 59.62 | 3.81  | 9.44   | 11.59 | 1.38  |
| Pyrite     | 0.07  | 0.01 | 5.00 | 1.15   | 2.61  | 0.20  | 4.41   | 10.21 | 1.46  |
| Albite     | --    |      | 2.62 | 12.08  | 14.31 |       | 0.94   | 1.14  |       |
| Mannardite | 22.60 | 0.53 | 4.28 | 0.46   | 0.88  | 20.98 | 0.59   | 1.17  | 51.71 |
| Actinolite | --    |      | 3.07 | --     |       |       | 0.40   | 0.57  |       |
| Apatite    | --    |      | 1.74 | 0.45   | 0.36  |       | 0.17   | 0.13  |       |
| Monazite   | --    |      | 5.26 | 0.00   | 0.01  |       | 0.01   | 0.02  |       |
| Kaolinite  | --    |      | 2.63 | 0.09   | 0.10  |       | 0.01   | 0.01  |       |
| Zircon     | --    |      | 4.71 | 0.00   | 0.01  |       | 0.00   | 0.01  |       |
| Carbon     |       |      | 1.05 | 29.49  | 14.03 | 74.60 | 39.22  | 19.08 | 40.12 |
| Total      |       |      |      | 100.00 |       |       | 100.00 |       |       |

**Note:**  $V_2O_5\#$  is the obtained by EPMA in table 1, and total  $V_2O_5$  is got by whole-rock chemical composition in table 3; Steps of calculating proportion of vanadium from each mineral: 1) translate the minerals volume fraction in TIMA results to mass fraction (X) by the equation:  $X_a = D_a \times V_a \div \sum_{1-n} D_n \times V_n$ .  $X_a$  = mineral<sub>a</sub> mass fraction,  $D_a$  - mineral<sub>a</sub> density,  $V_a$  - mineral<sub>a</sub> volume fraction, 1-n: minerals in the ore,  $D_n$  - mineral<sub>n</sub> density;  $V_n$  - mineral<sub>n</sub>; 2) obtain the  $V_2O_5$  mass (M) of each mineral by  $M_a = X_a \times m_a$ ,  $M_a$  -  $V_2O_5$  mass of mineral<sub>a</sub>,  $m_a$  -  $V_2O_5$  content of mineral<sub>a</sub> by EPMA ;3) calculate the proportion (P) of vanadium from each mineral by the equation:  $P_a = M_a / M_{ore}$ ,  $P_a$  – proportion of vanadium from mineral<sub>a</sub>,  $M_{ore}$  - total mass of vanadium in the ore rock. Density data of minerals are from IMA Database of Mineral Properties, available: <https://rruff.info/ima/>.

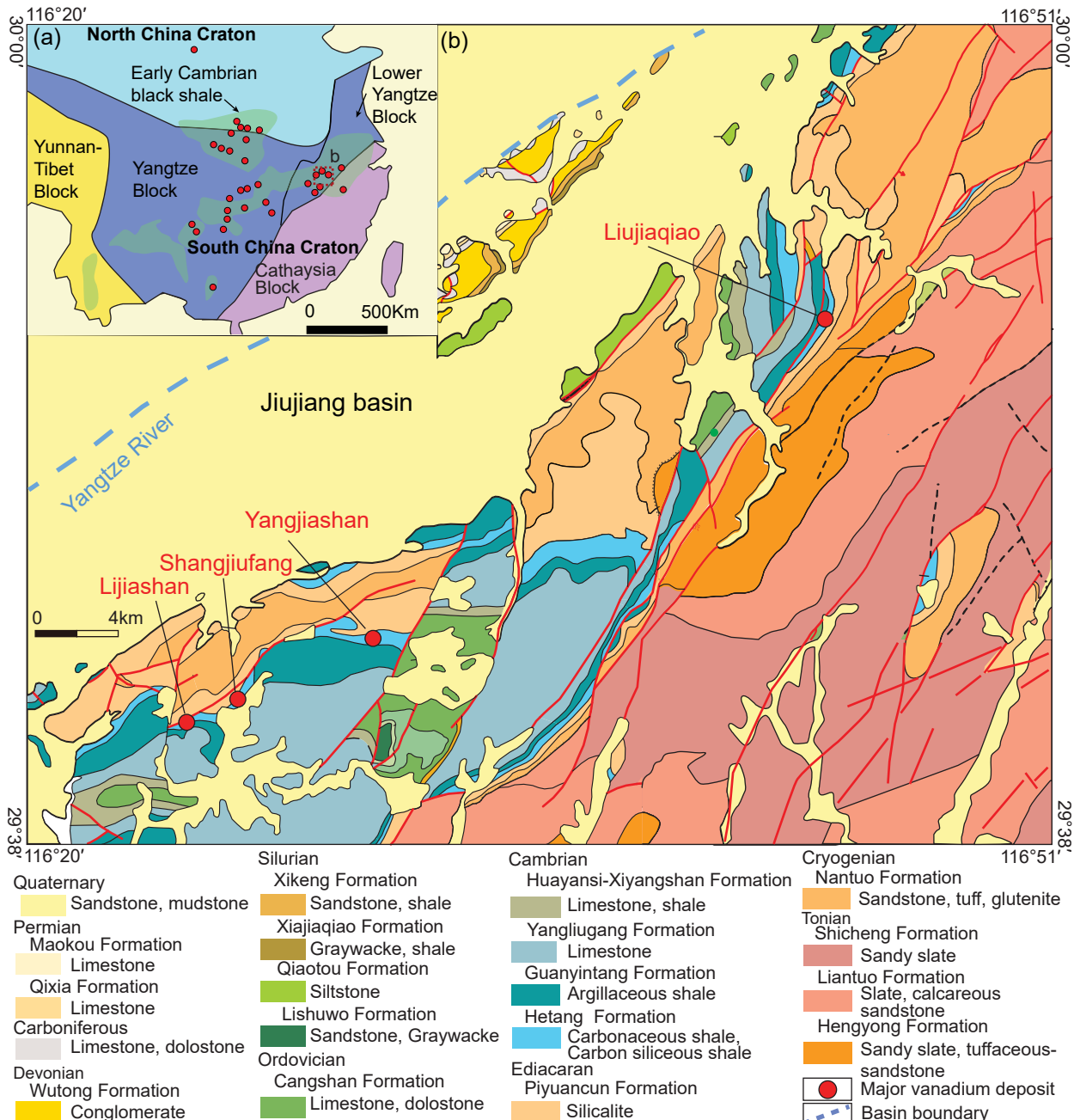


Fig. 1

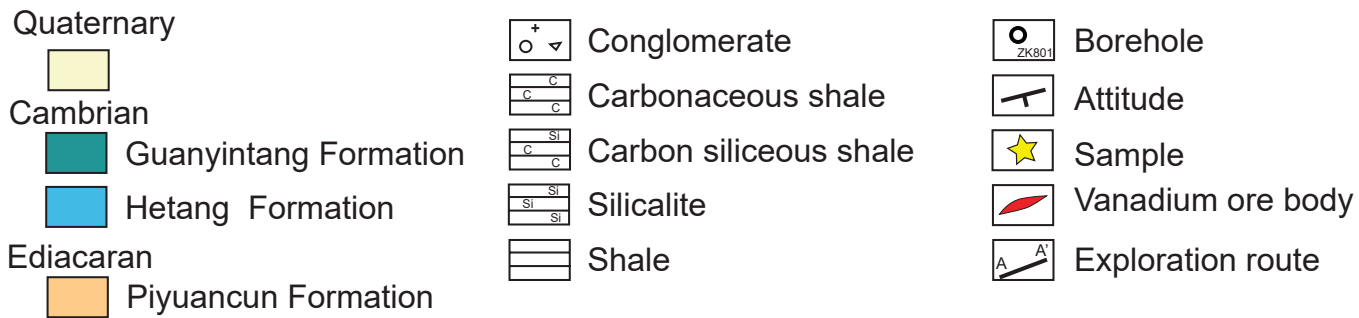
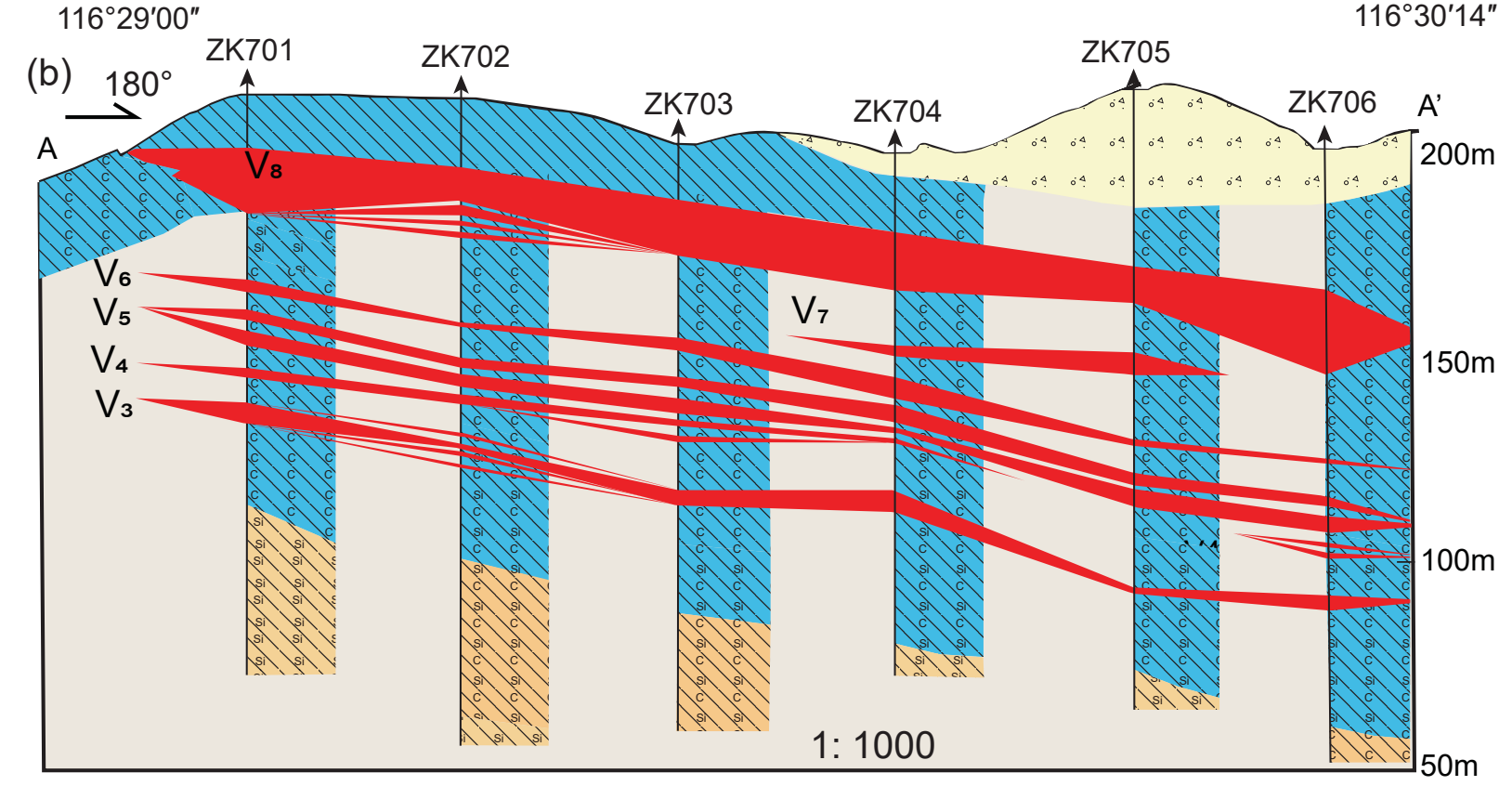
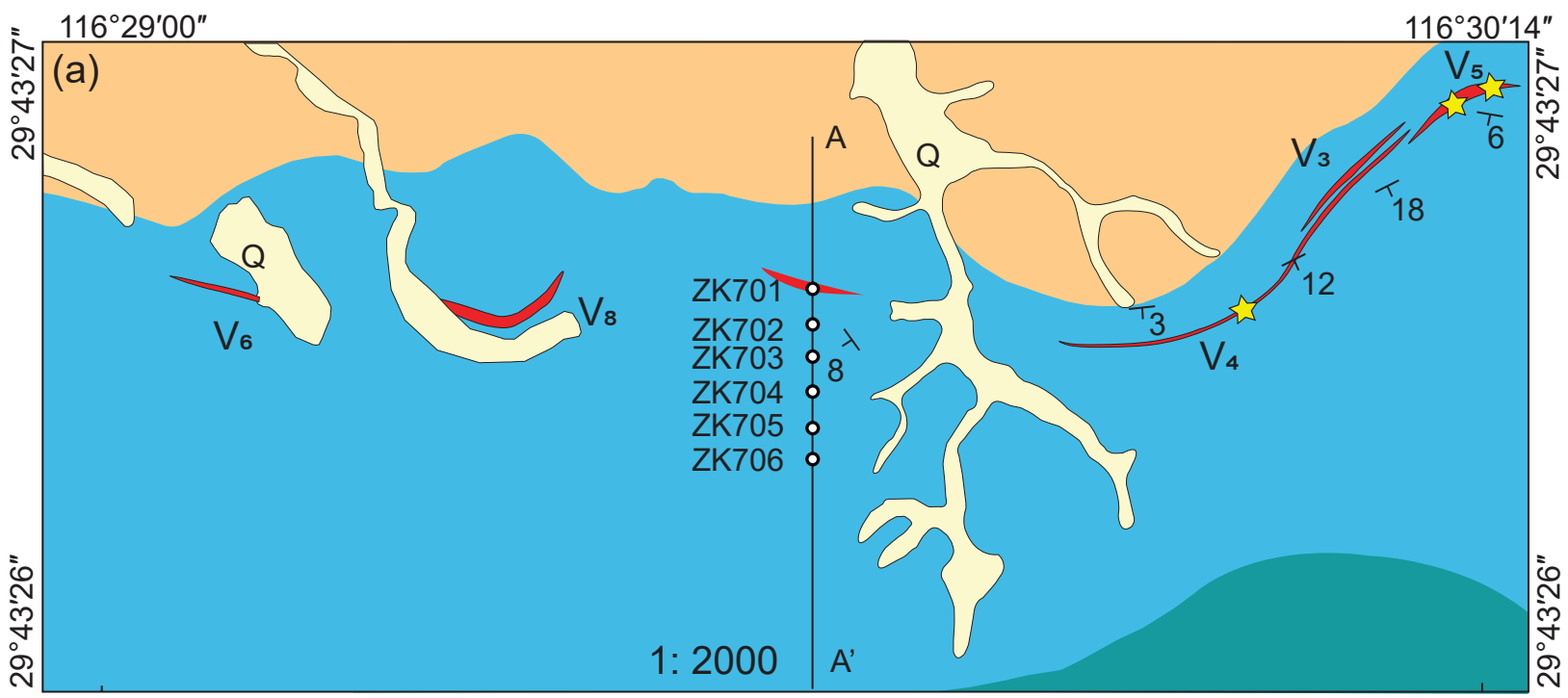
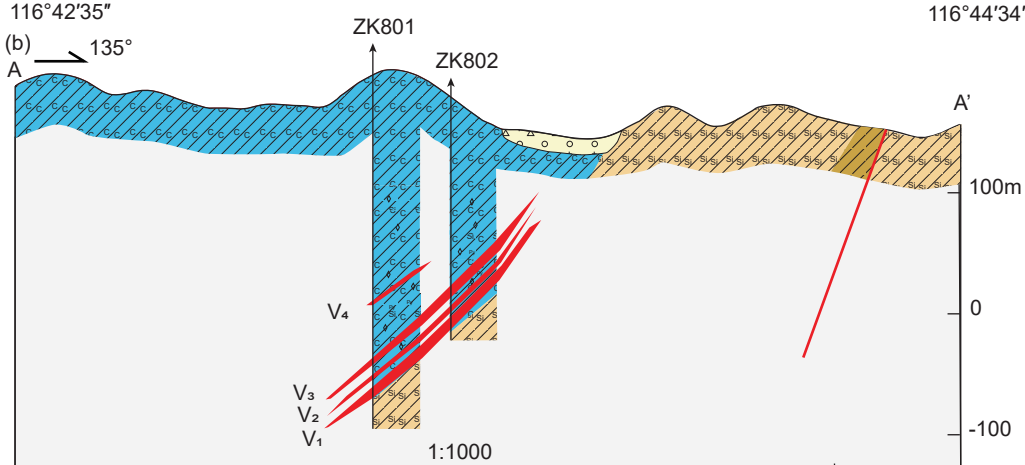
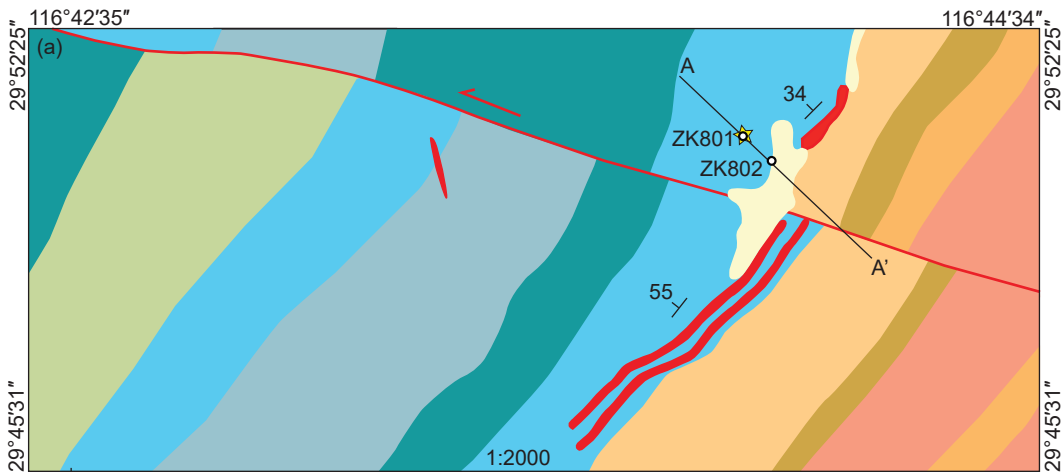


Fig. 2



Quaternary



Cambrian

Xiyangshan Formation

Huayansi Formation

Yangliugang Formation

Guanyintang Formation

Hetang Formation

Ediacaran

Piyuancun Formation

Doushantuo Formation

Cryogenian

Nantuo Formation

Tonian

Liantuo Formation

Conglomerate

Carbonaceous shale

Carbon siliceous shale

Silicalite

Shale

Borehole

Carbonatation / pyrite-bearing

Vanadium ore body

Exploration route

Fault

Attitude

Sample

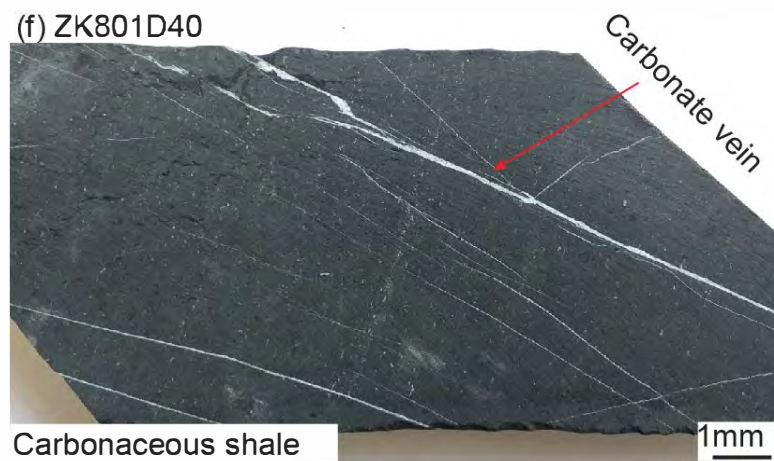
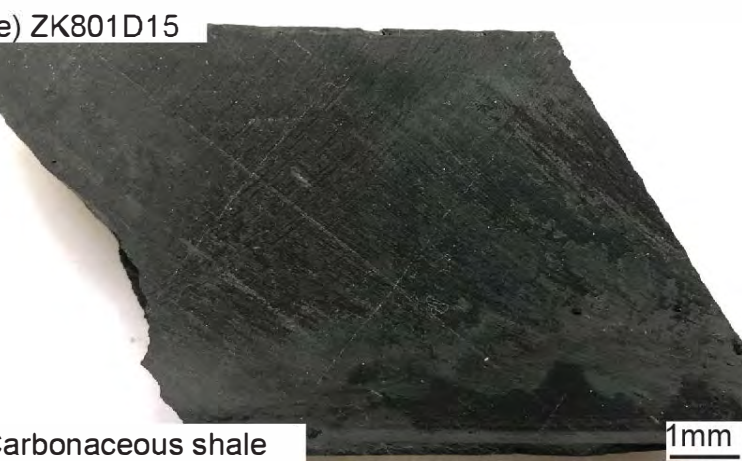
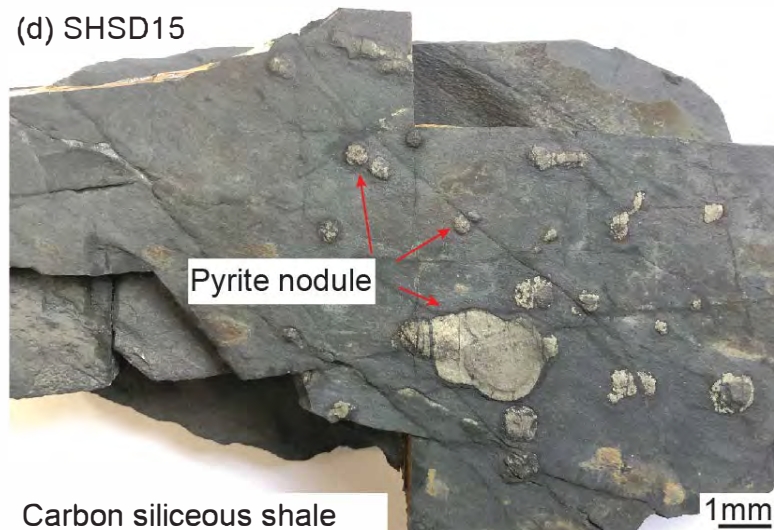
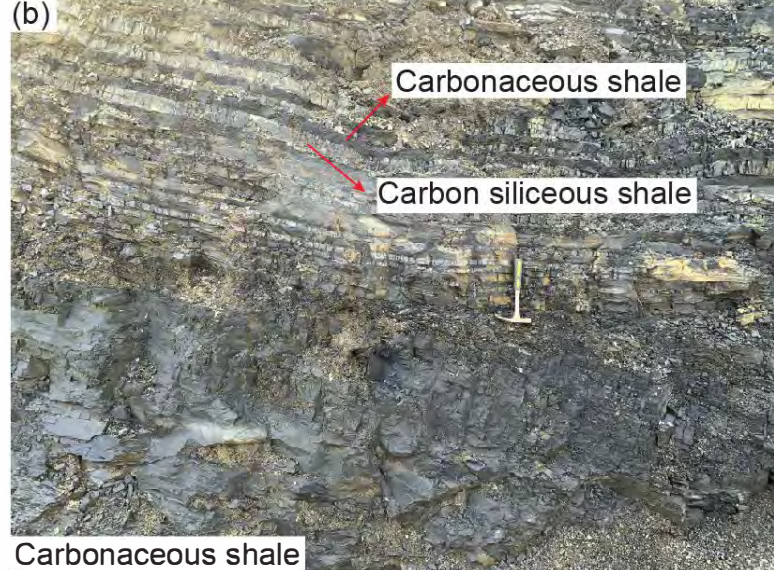
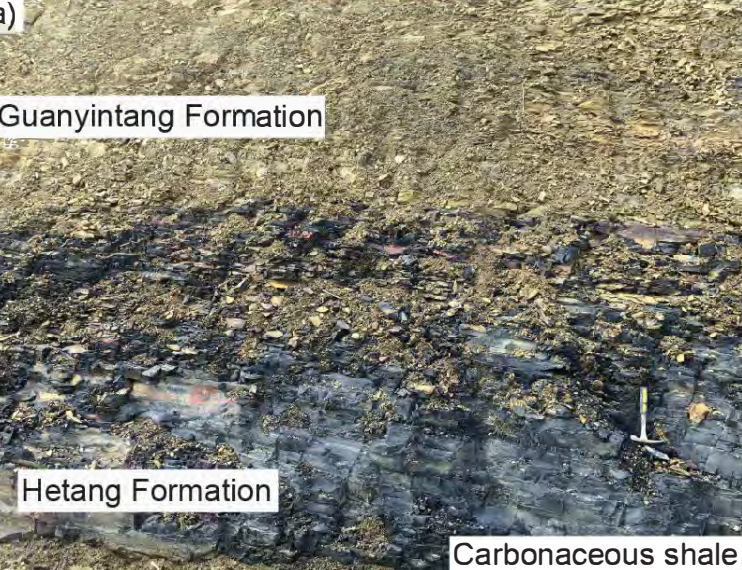


Fig. 4

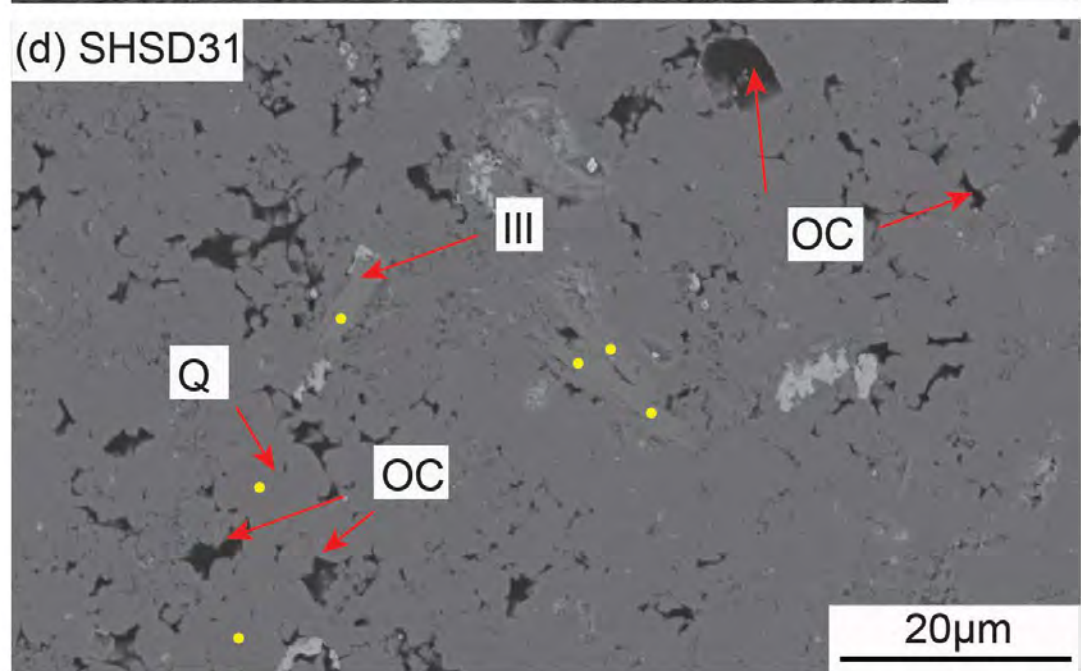
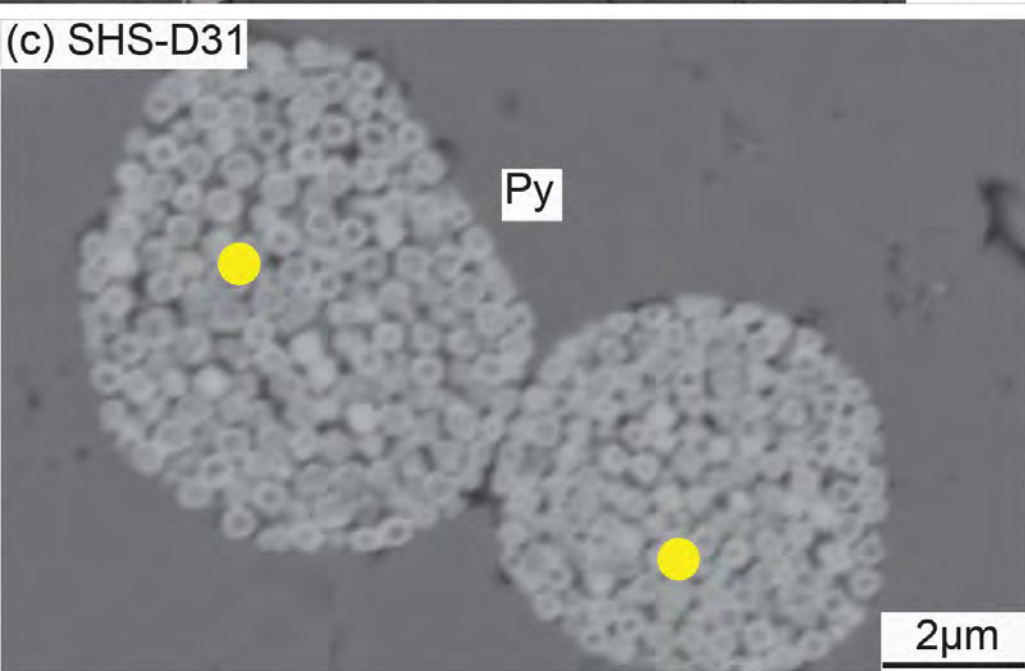
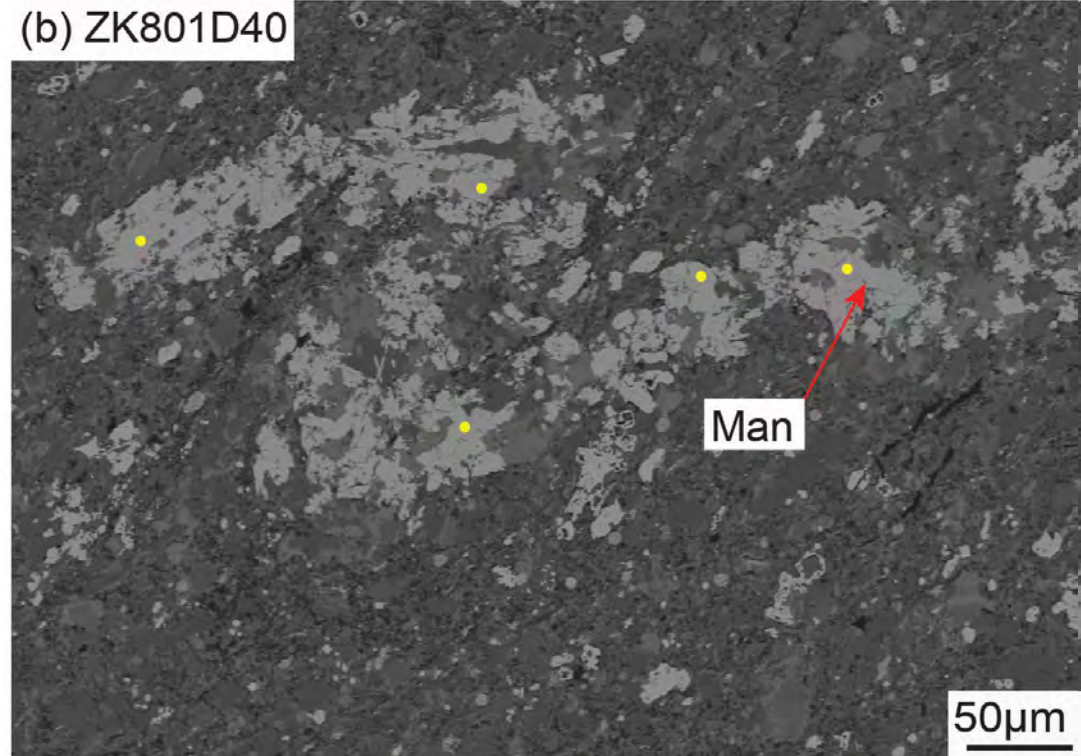
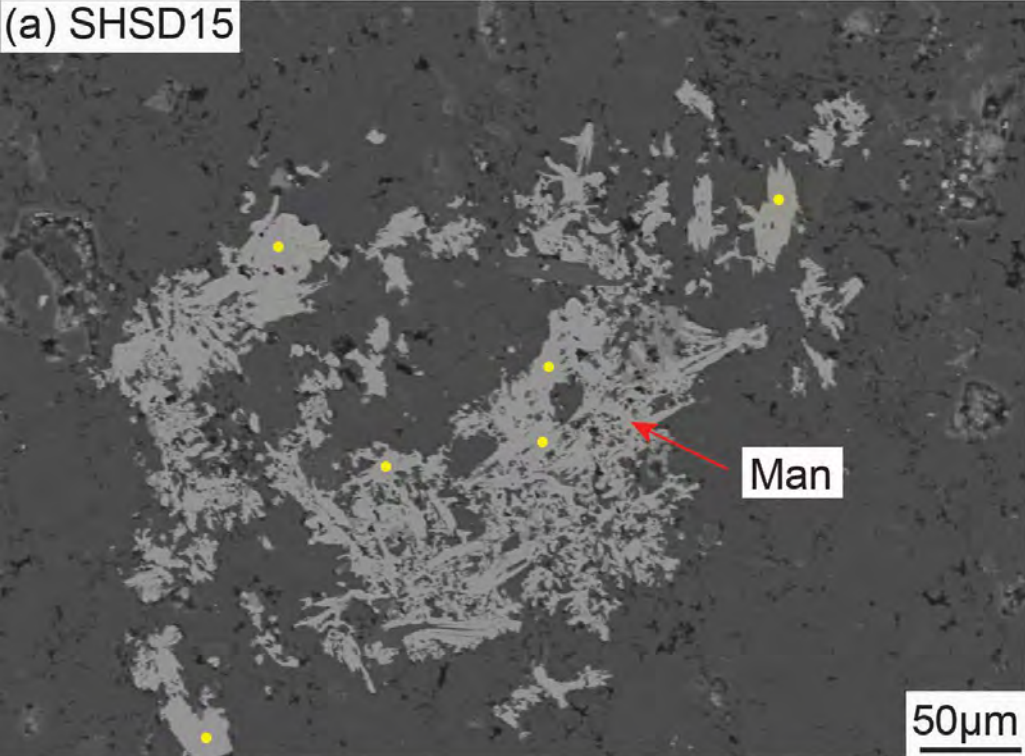
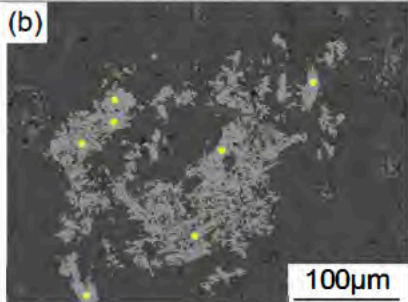
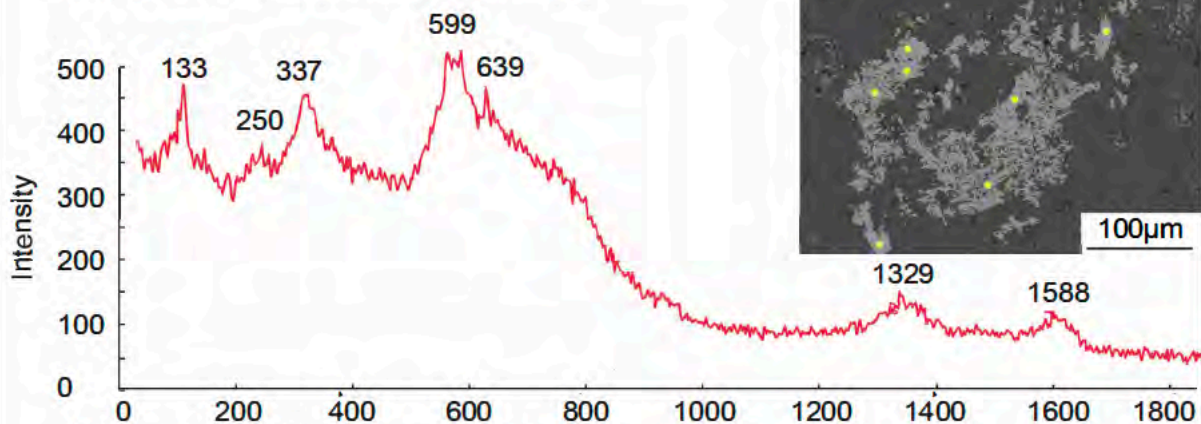


Fig. 5

(a) V-Ti-Ba oxide in this research (532nm)



(c) Raman spectrum of mannardite from IMA (532nm)

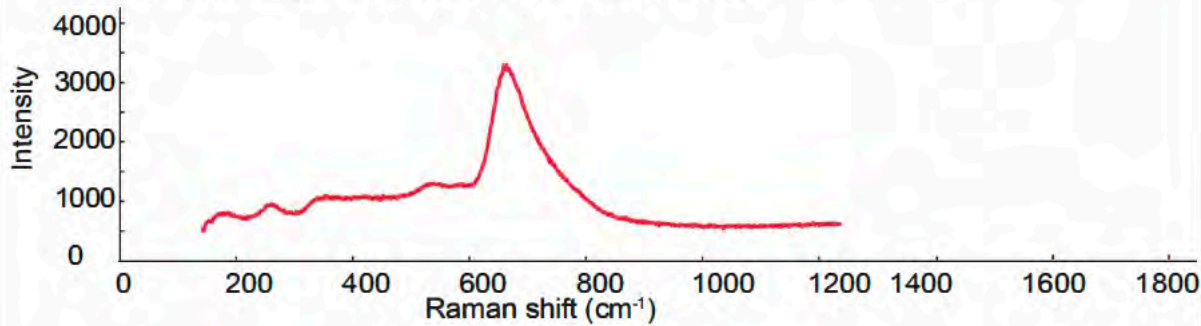


Fig. 6

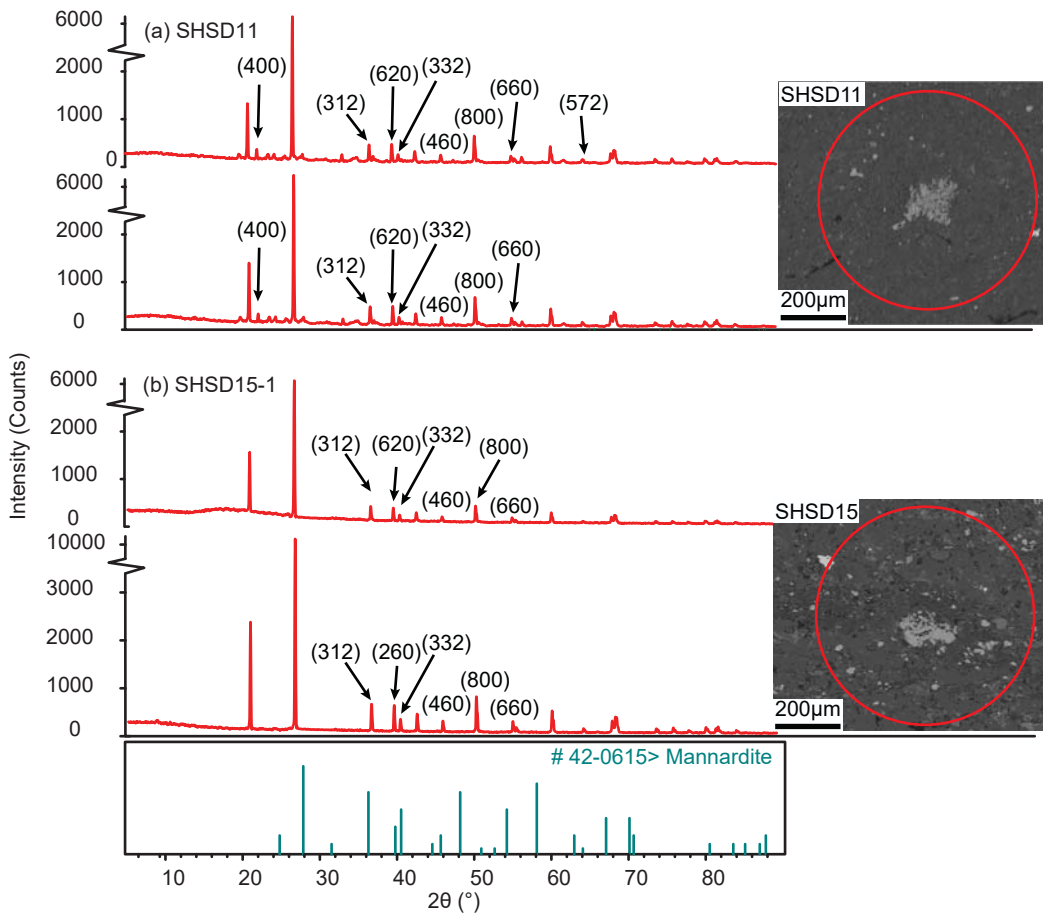


Fig. 7

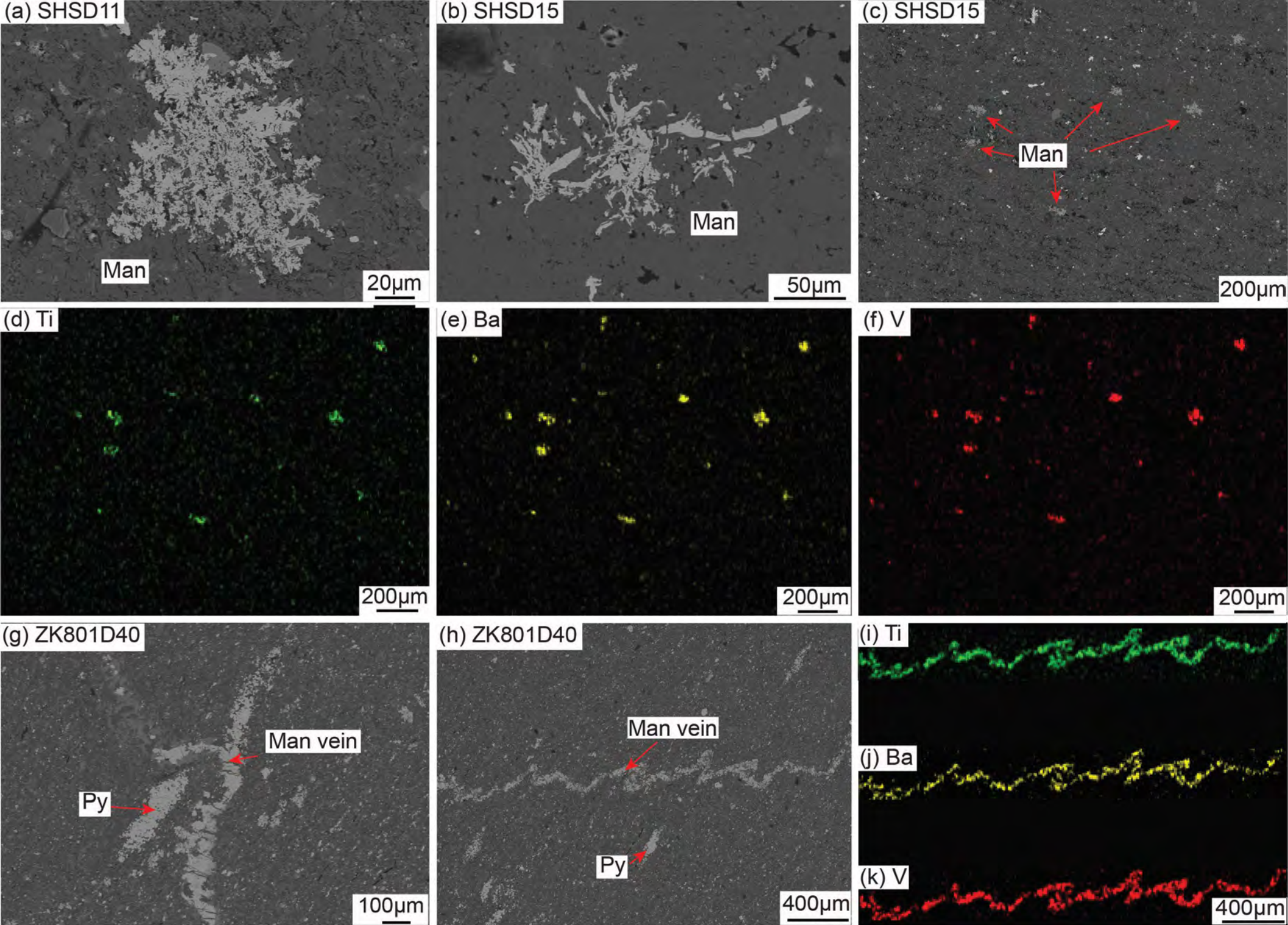


Fig. 8

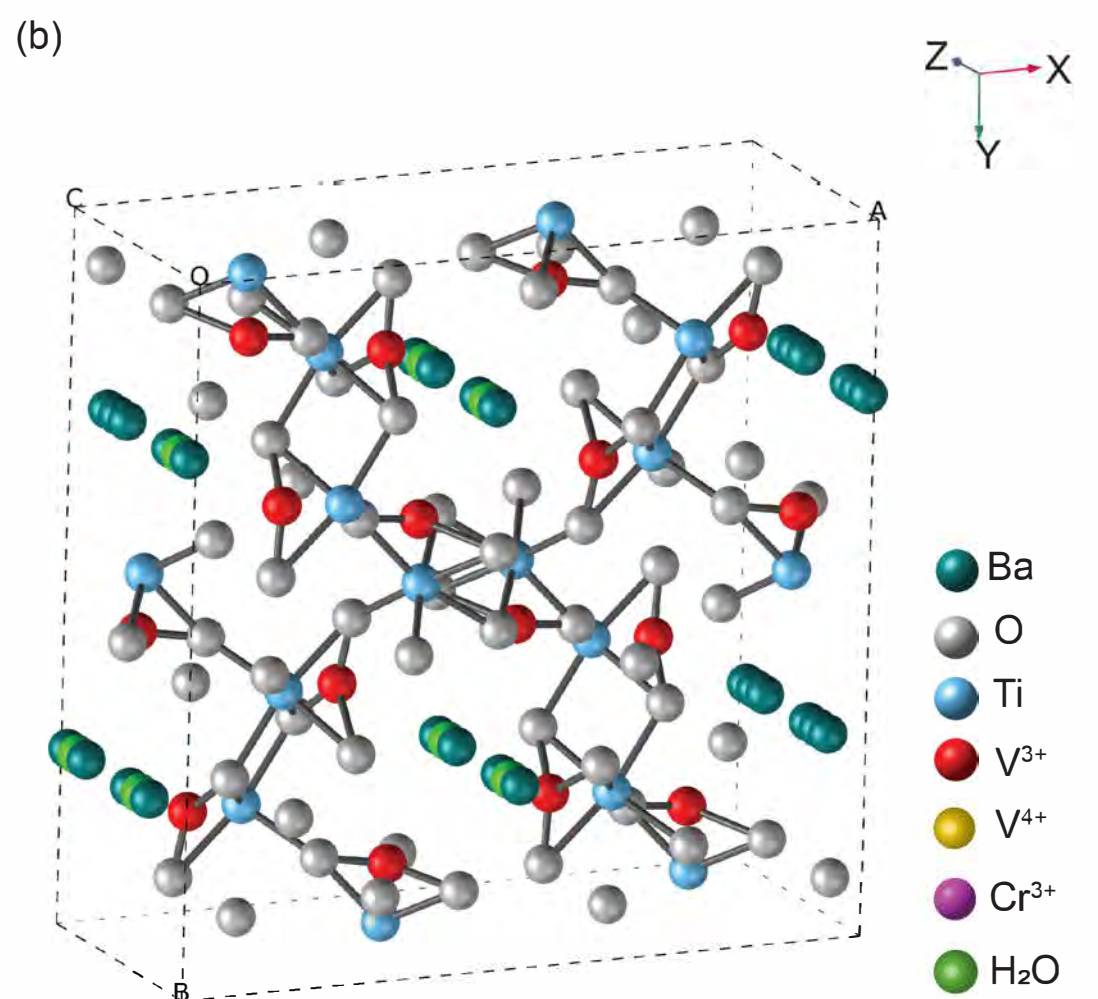
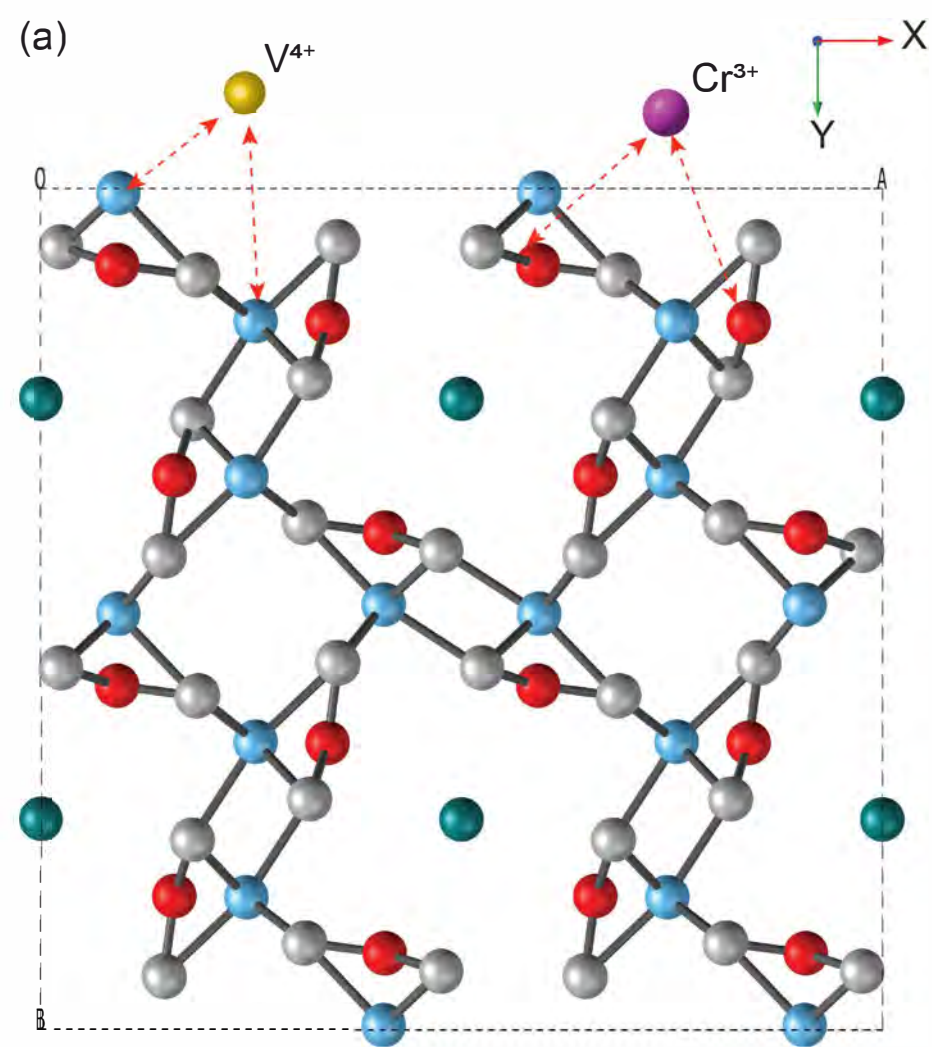


Fig. 9

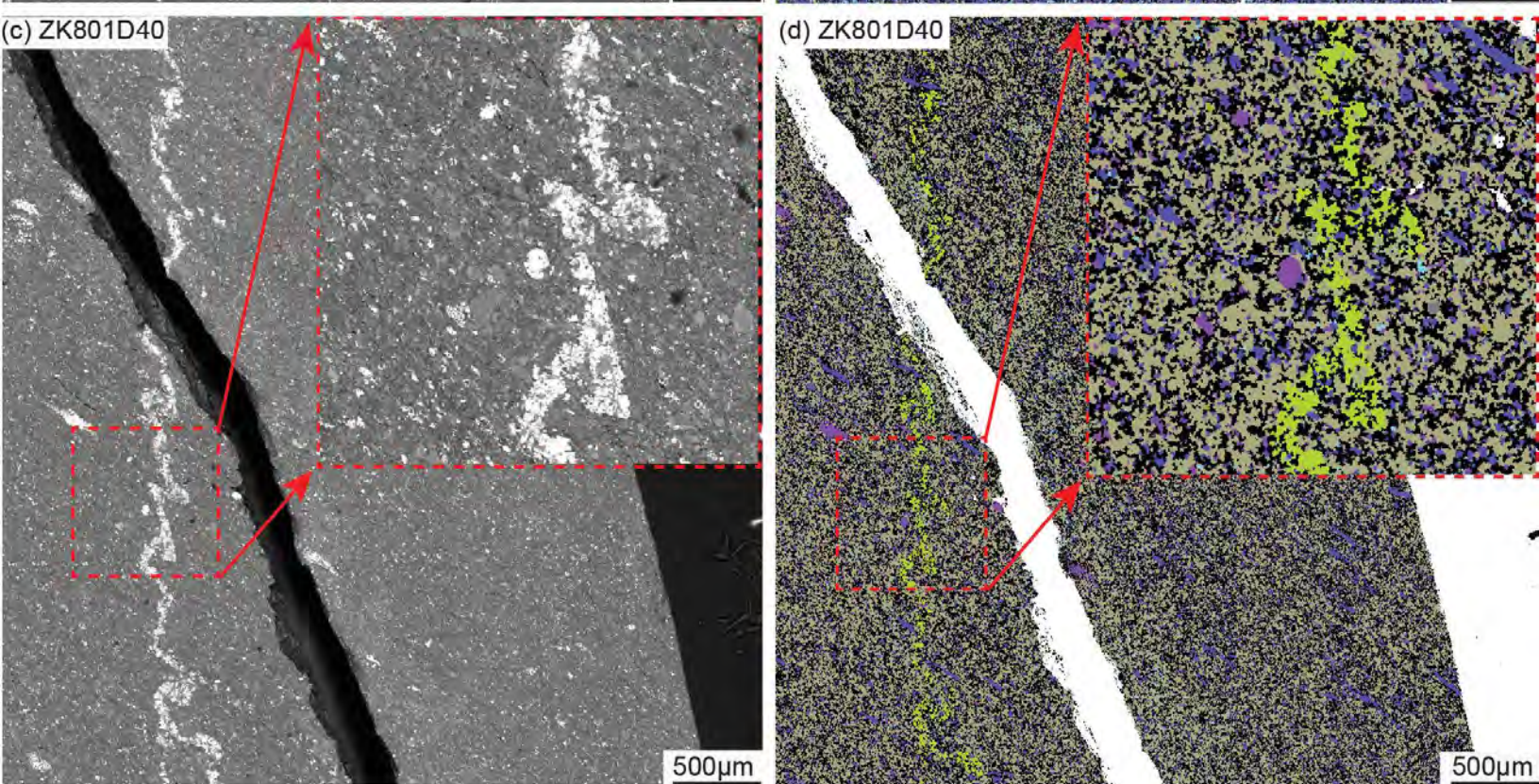
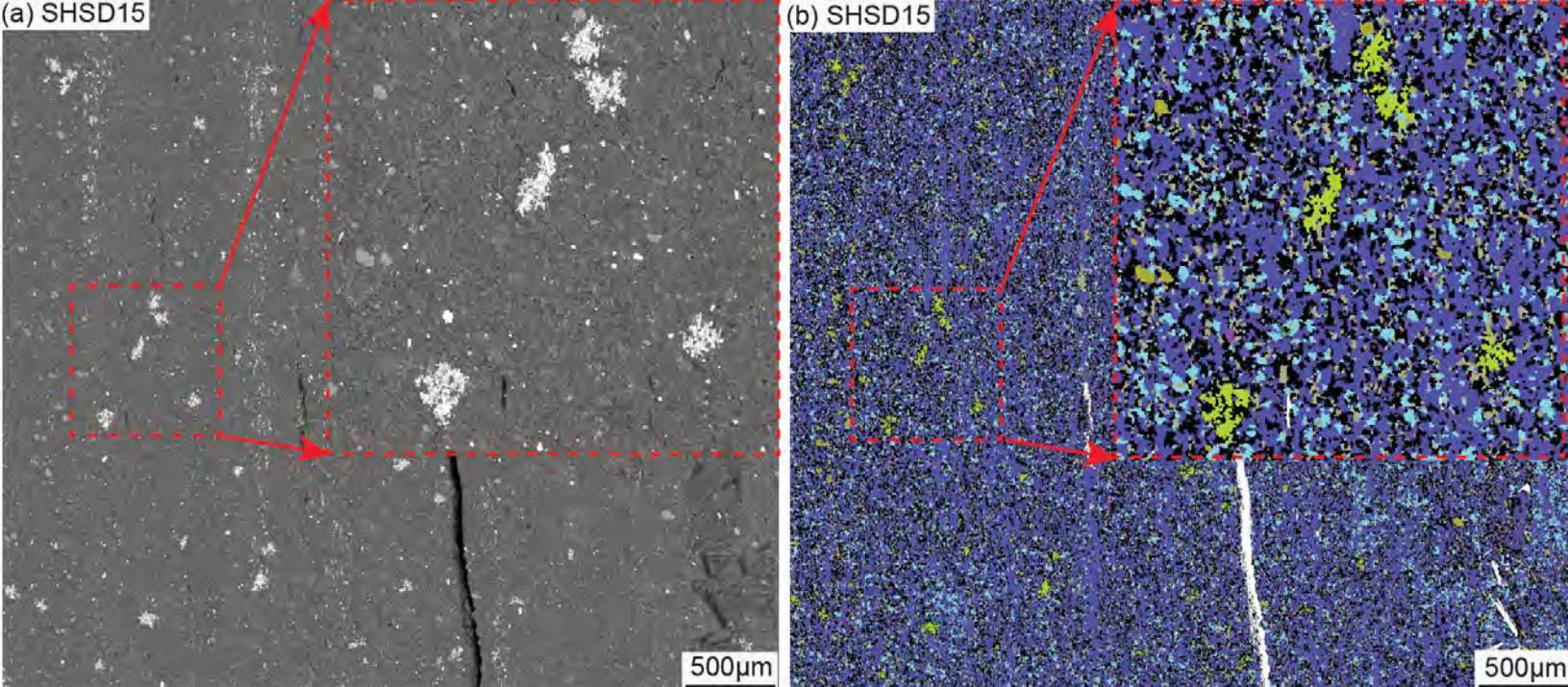


Fig. 10

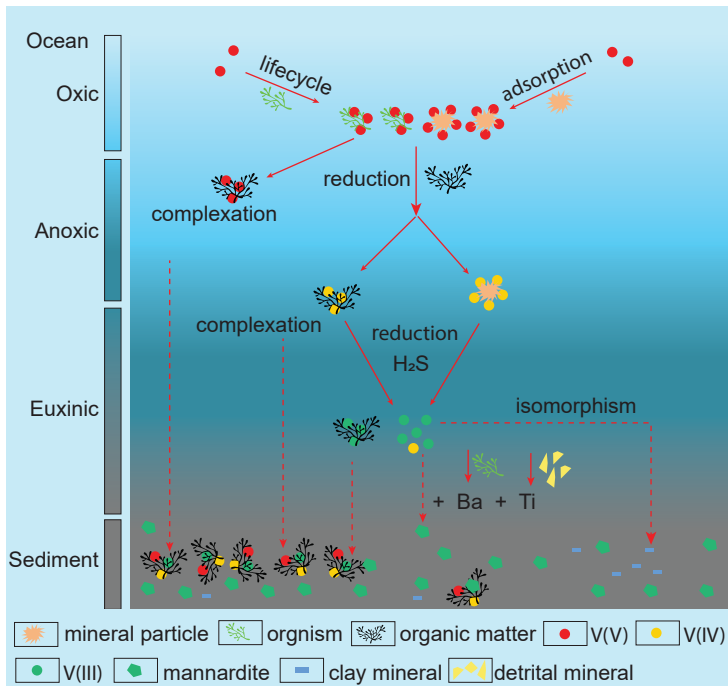


Fig.11